



Lithospheric- and crustal-scale controls on variations in foreland basin development in the Northern Alpine Foreland Basin

Lucas H.J. Eskens^{a,*}, Nevena Andrić-Tomašević^a, Peter M. Süß^b, Matthias Müller^c, Rolf Herrmann^c, Todd A. Ehlers^{b,d}

^a Karlsruhe Institute of Technology, Institute of Applied Geosciences, Karlsruhe, Germany

^b University Tübingen, Department of Geosciences, Tübingen, Germany

^c ONEO GmbH & Co. KG, Hannover, Germany

^d University of Glasgow, School of Geographical and Earth Sciences, Glasgow, UK

ARTICLE INFO

Keywords:

Pro-foreland basin
Flexure
Eocene
Oligocene
Early Miocene
Molasse Basin

ABSTRACT

The Northern Alpine Foreland Basin (*i.e.*, Molasse Basin) developed due to flexural subsidence from slab- and topographic loading during continental collision between the Adriatic and European plates. Previous studies highlight a diachronous transition from underfilled- to overfilled conditions in the Molasse Basin in response to orogen-parallel variations in flexural subsidence and sediment supply. In this contribution, we investigate the lithospheric- and crustal-scale orogenic process(es) that generated this diachronous transition. For this, we conducted a tectonostratigraphic analysis of the Molasse Basin. Firstly, we constructed a 3D geological model to derive the architecture of the European margin during the Eocene onset of flexure. Second, 2D/3D reflection seismic- and borehole data were used to characterise the spatiotemporal development of depositional environments and syn-flexural normal fault kinematics in the German Molasse. Our data show a stepwise rather than continuous eastward migration of the underfilled- to overfilled transition. Furthermore, syn-flexural fault kinematics document a Rupelian to early Burdigalian northward younging trend and higher cumulative Cenozoic offsets in the Eastern German Molasse (< 230 m) compared to the Western German Molasse (< 150 m). This implies a west-to-east increase in the curvature of bending of the European plate, induced by along-strike variations in the magnitude of applied loads and/or European lithospheric strength variations. These variations drove lateral variations in accommodation space and sediment supply. Subsequently, this led to the diachronous underfill-to-overfilled transition in the Molasse Basin. Taken together, we suggest that the diachronous transition was driven by spatiotemporal variations in the thickening of the orogenic wedge supported by slab detachment, promoted by subduction- and collision of the irregular European margin.

1. Introduction

Flexural basins develop next to orogens as a result of topographic and subsurface loading (such as deep-seated loads or subducting slabs) that result in lithospheric flexure of the subducting foreland plate (Beaumont, 1981; Flemings and Jordan, 1989; DeCelles and Giles, 1996; Sinclair, 1997a; Roure, 2008). Their stratigraphic fill and basin architecture record the interplay between the flexural generation of accommodation space and sediment supply from the adjacent mountain range (Flemings and Jordan, 1990; DeCelles and Giles, 1996). Numerous foreland basins (*e.g.*, Appalachian, Apenninic, and Tarim, Lash, 1988; He *et al.*, 2016; Amadori *et al.*, 2019) record along-strike variations in

basin architectures (*e.g.*, coeval existence of both underfilled and overfilled deposition, *sensu* Homewood *et al.*, 1986). Several processes can produce along-strike variable foreland basin architectures. Examples include orogen-parallel variations in crustal thickening of the orogenic wedge (Whiting and Thomas, 1994; DeCelles and Mitra, 1995), lateral slab tearing (Meulenkamp *et al.*, 1996; Van der Meulen *et al.*, 1998; Ascione *et al.*, 2012), climate change and/or sediment availability (Kuhlemann and Kempf, 2002; Schlunegger and Castellort, 2016; Malkowski *et al.*, 2017; Garefalakis and Schlunegger, 2019), and along-strike variations in the inherited pre-foreland crustal architecture (Dewey and Kidd, 1974; Cooper *et al.*, 1995; Sinclair, 1997a; Roure, 2008). A natural example that records along-strike variations in the

* Corresponding author.

E-mail address: lucas.eskens@kit.edu (L.H.J. Eskens).

<https://doi.org/10.1016/j.tecto.2024.230283>

Received 10 May 2023; Received in revised form 17 March 2024; Accepted 18 March 2024

Available online 25 March 2024

0040-1951/© 2024 The Authors. Published by Elsevier B.V. This is an open access article under the CC BY-NC license (<http://creativecommons.org/licenses/by-nc/4.0/>).

stratigraphic basin architecture is the Northern Alpine Foreland Basin (e.g., Kuhlemann and Kempf, 2002, hereafter referred to as the Molasse Basin, MB, Fig. 1). To better understand the controls of lithospheric- and crustal-scale processes on the along-strike variation in MB architecture, we investigate the tectonostratigraphic evolution of this basin and relate it to the geodynamic evolution of the Alps.

Since the Late Cretaceous, the European and Adriatic plates have been converging (e.g., Handy et al., 2015). By the late Eocene, convergence led to continental collision and the onset of flexural subsidence of the peripheral MB (e.g., Schmid et al., 1996). A key characteristic of the Cenozoic syn-flexural basin fill is the Oligocene to early Miocene diachronous transition from underfilled- to overfilled deposition (i.e., transition from flysch to molasse deposition; Homewood and Lateltin, 1988; Lemcke, 1988; Allen et al., 1991; Bachmann and Müller, 1991; Sinclair, 1997a; Kuhlemann and Kempf, 2002). This transition started at 31.5 to 30 Ma in the Swiss Molasse (Schlunegger et al., 1997b; Kempf et al., 1999; Kempf and Pross, 2005) and reached the Austrian Molasse by 19 to 18 Ma (Hülscher et al., 2019). The mechanisms proposed for this diachronous transition include eustasy (Bachmann and Müller, 1991; Jin et al., 1995; Zweigel et al., 1998, Eastern German Molasse), inherited basement architecture (stratigraphy and structures, Lihou and Allen, 1996, Swiss Molasse), visco-elastic relaxation of the European plate (Zweigel et al., 1998; Hülscher et al., 2019; Borzi et al., 2022, Eastern German and Austrian Molasse), and slab breakoff (Sinclair, 1997a; Schlunegger and Kissling, 2015; Schlunegger and Castellort, 2016, Swiss Molasse). On the scale of the entire MB, Alpine lithospheric-scale processes may have governed along-strike variations in sediment supply, driving the along-strike diachronous underfill- to overfill transition (Kuhlemann and Kempf, 2002; Schlunegger and Kissling, 2022). In addition, it has been suggested that lateral tearing of the European slab governed west-to-east decenter migration along the entire Alpine-Carpathian chain (Meulenkamp et al., 1996). This slab breakoff and tearing hypothesis explains the mechanisms that induced the diachronous underfill- to overfilled transition in the MB during the Oligocene to early Miocene. Fingerprints of lateral slab tearing include lithospheric-scale STEP faults (*sensu* Govers and Wortel, 2005; Neely and Furlong, 2018; Andrić-Tomašević et al., 2023), a younging trend of asthenospheric magmatism parallel to the proposed direction of slab tearing (Ferrari, 2004; Ferrari et al., 2012; Menant et al., 2016), and trench-mountain curvature (Li et al., 2013; Andrić-Tomašević et al., 2023). However, such features are less evident in the Alps. Therefore, alternative mechanisms, which may have controlled the Oligocene to early Miocene evolution of the MB, require consideration.

Previous paleogeographic reconstructions suggest an irregular European passive margin (Stampfli, 1993; Faupl and Wagreich, 2000; Stampfli et al., 2002; Ziegler and Dèzes, 2007; Handy et al., 2010; Handy et al., 2015). This irregularity was characterised by the presence of the continental Briançonnais terrane, which tapered out between the future Western/Central- and Eastern Alps (Faupl and Wagreich, 2000; Mohn et al., 2010; Rosenberg et al., 2021). Previous geologic (Alps, Stockmal et al., 1987; Mohn et al., 2014; Manatschal et al., 2022; Zagros mountains, Alipour, 2023) and geodynamic studies (van Hunen and Allen, 2011; Tetreault and Buitter, 2012; Vogt and Gerya, 2012) demonstrated that subduction- and collision of an irregular margin leads to orogen-parallel variations in the foreland basin architecture (Lash, 1988; Gül et al., 2015; Angrand et al., 2018). However, the influence of a subducting irregular European margin on the MB architecture has received little attention and focused mostly on the Swiss Molasse only. (Lihou and Allen, 1996; Sinclair, 1997a; Schlunegger and Kissling, 2022). The irregularity of the European margin promoted an earlier collision in the western part of the European-Adria suture (also inferred by Schlunegger and Kissling, 2022). If true, this led to an earlier underfill-to-overfill transition in the western part of the MB compared to the eastern part. In this contribution, we evaluate both the hypotheses that the diachronous underfill-to-overfill transition in the MB was controlled by 1) slab breakoff- and tearing or 2) collision- and subduction of the irregular

European passive margin.

To test these hypotheses, we construct a 3D geological model of the MB north of the present-day Alpine thrust front using existing subsurface models (GeoMol, 2015; Fig. 1a). Furthermore, we interpret 2D/3D seismic data in the German Molasse (Fig. 1a, 2D seismic lines and seismic volumes A and B) for the late Eocene to early Miocene depositional environments and syn-flexural normal fault kinematics. Combining these analyses enables a reconstruction of the tectonostratigraphy of the MB resulting from the geodynamic evolution of the Alps. Our results suggest that the pre-flexural European passive margin architecture controlled the late Eocene architecture of the German Molasse. Furthermore, subduction- and collision of the irregular European margin likely influenced the along-strike variations in the surface uplift of the Alps, subsequently resulting in basin-parallel variations in sediment availability.

2. Geological setting

The Alps and the adjacent MB extend from south of Lake Geneva to Lower Austria, striking roughly *E-W* over ca. 700 km (Fig. 1). From west to east, the MB is bounded north by the Jura Mountains, the Swabian/Franconian Alb, and the Bohemian Massif. The thickness of the syn-flexural Cenozoic fill of the MB increases from north to south, reaching ~5000 m in front of the Alps (e.g., Bachmann and Müller, 1991). A rough division of the MB is typically made between the Oligocene brackish/terrestrial Western Molasse (Swiss and Western German Molasse, Fig. 1a) and littoral to bathyal Eastern Molasse (Eastern German and Austrian Molasse, Fig. 1a, Kuhlemann and Kempf, 2002). Furthermore, we subdivide the Eastern Molasse into the Eastern German Molasse (German Molasse east of Munich) and Austrian Molasse (Fig. 1a) because of their different histories (Subsection 2.2).

The adjacent Alps are a nappe stack of European and Adriatic-derived material (e.g., Schmid et al., 1996; Schmid et al., 2004a). While European-derived units dominate the western part of the orogen, Adriatic-derived units are more prominent in the eastern part (Fig. 1b). This lateral variation in the structure of the nappe stack suggests orogen-parallel variations in Alpine tectonics (e.g., Schmid et al., 1996; Stampfli et al., 1998; Handy et al., 2010).

2.1. Geodynamic evolution of the Alpine hinterland

The Penninic domain (Piemont Ocean and Valais Through) separated the Adriatic and European plates from the Late Jurassic until Late Eocene continental collision (Schmid et al., 1996; Ziegler et al., 1996; Mohn et al., 2010; Le Breton et al., 2021). Along the future Western and Central Alps, the Piemont Ocean and Valais Trough were separated by the continental Briançonnais terrane (Handy et al., 2010; Mohn et al., 2010; Le Breton et al., 2021; Rosenberg et al., 2021). However, this terrane tapered out towards the future Eastern Alps (e.g., Stampfli, 1993; Stampfli et al., 2002). This led to an irregular European margin. Subduction of the Penninic domain started in the Late Cretaceous (84 Ma, Stampfli et al., 1998; Handy et al., 2010; Handy et al., 2015; Le Breton et al., 2021). By the late Eocene, continental collision started (Schmid et al., 1996; Ziegler et al., 1996), leading to the overthrusting of the European margin by the Alpine nappe stack. Alpine nappe stacking and European slab loading caused flexural subsidence of the foreland (Allen et al., 1991; Schmid et al., 1996; Wagner, 1998). At that time, the shelf sediments of the Ultrahelvetian domain were incorporated into the thrust wedge to form the Helvetic nappes (Burkhard, 1988; Pfiffner, 1993; Schmid et al., 1996). Coeval late Eocene to early Oligocene emplacement of intrusives along the Periadriatic Fault (Fig. 1b, Dal-Piaz et al., 1988; Barth et al., 1989; von Blanckenburg and Davies, 1992) suggests that continental collision was followed by European oceanic slab breakoff (~43–30 Ma, von Blanckenburg and Davies, 1995; Schmid et al., 1996). This led to an increase in exhumation, backthrusting, and low-angle detachment faulting in the Western/Central Alps, which

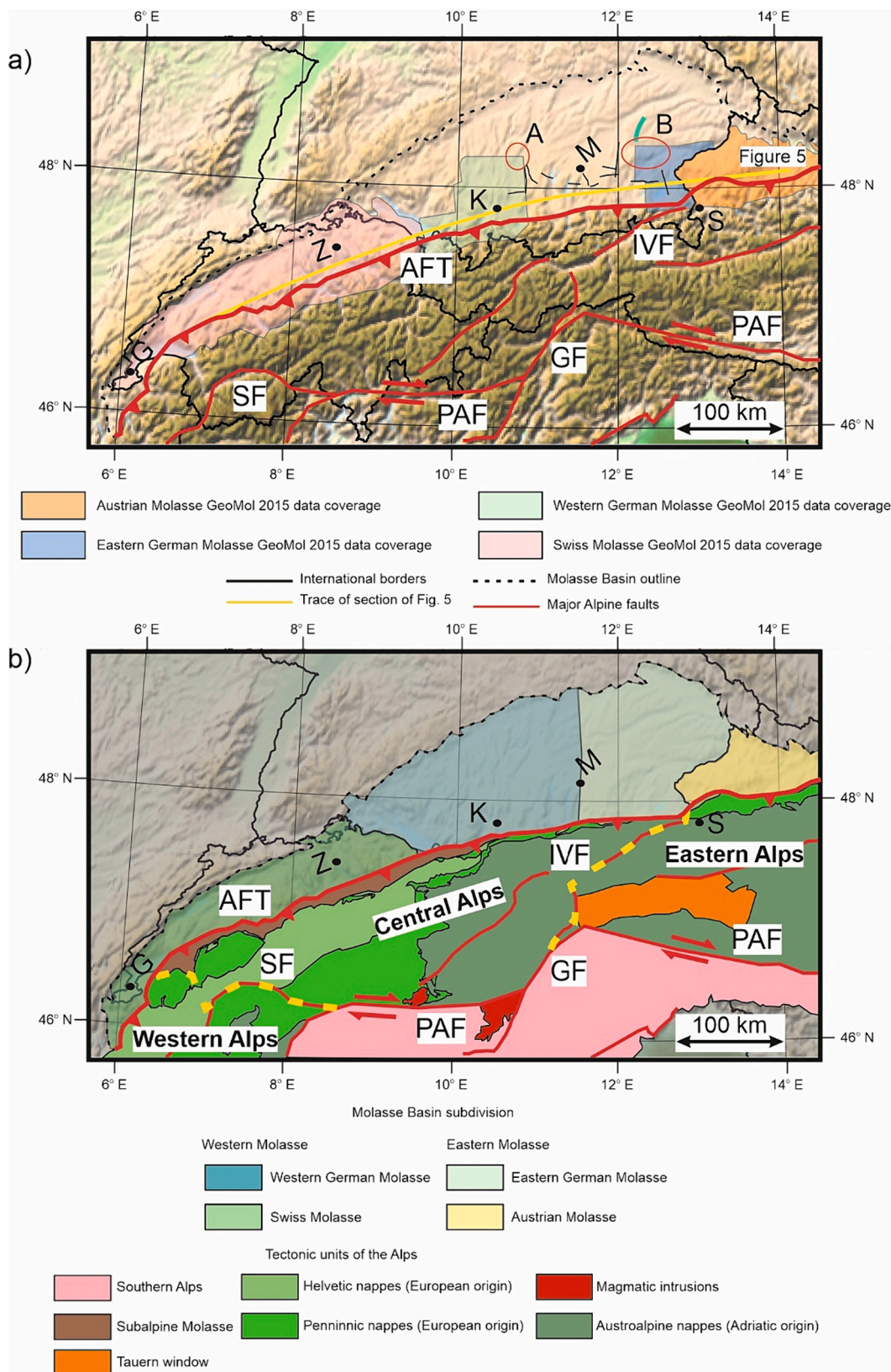


Fig. 1. a) Relief map of the Alps, Molasse Basin, and surrounding areas from the ETOPO1 Global Relief Model (Amante and Eakins, 2009), showing the locations of data and model results presented in this study. The red circles indicate the locations of 3D seismic volumes A and B, and the black lines are 2D seismic lines. The green line north of seismic volume B shows the location of the seismic line shown in Fig. A14. b) Tectonic map of the Alps and Molasse Basin, indicating the subdivision used in this study. Tectonic units in the Alps are modified from (Schmid et al., 2004b). The subdivision of the Alps is based on (Kuhlemann and Kempf, 2002), where the yellow dashed lines indicate the borders between different parts of the orogen. The subdivision of the Molasse Basin is based on differences in the tectonostratigraphic development of various parts of the basin (See Subsection 2.2.2 for details). AFT = Alpine Frontal Thrust, GF = Giudicarie Fault, SF = Simplon Fault, PAF = Periadriatic Fault, IVF = Inntal Valley Fault, G = Geneva, K = Kaufbeuren, L = Linz, M = Munich, S = Salzburg, Z = Zürich.

further caused increased erosion rates between 30 and 20 Ma (Hurford, 1986; Schmid et al., 1996; Schlunegger and Willett, 1999; Von Eynatten et al., 1999; Schlunegger and Kissling, 2015). Despite slab breakoff, the Alpine nappes continued to migrate northward, overthrusting the Infralhelvetic domain by the early Oligocene (including the parautochthonous Cenozoic cover of the Aar Massif, consisting out of middle- to late Eocene limestones and early Oligocene flysch, Pfiffner, 1986; Allen et al., 1991; Pfiffner, 1993; Schmid et al., 1996; Heyng, 2012; Zerlauth et al., 2014). Along the Central- and Eastern Alpine front, the basal Helvetic thrust remained active until at least the late Oligocene (Schmid et al., 1996; Zerlauth et al., 2014). The thrust front of the

Eastern Alps continued to migrate northward during the Oligocene and early Miocene (Covault et al., 2009; Hinsch, 2013; Zerlauth et al., 2014).

A second slab breakoff is suggested below the Eastern Alps during the early Miocene (20 Ma, Schmid et al., 2004a; Ustaszewski et al., 2008; Handy et al., 2015). Similar to the late Eocene to early Oligocene breakoff, this breakoff event correlates with increased exhumation rates (Fügenschuh et al., 1997; Fox et al., 2016) and increased sediment supply from the Eastern Alps (Kuhlemann, 2000), as well as a switch from in-sequence to out-of-sequence thrusting (Hurford et al., 1989; Covault et al., 2009; Hinsch, 2013; Von Hagke et al., 2014; Ortner et al., 2015). However, continued indentation by the Adriatic plate resulted in

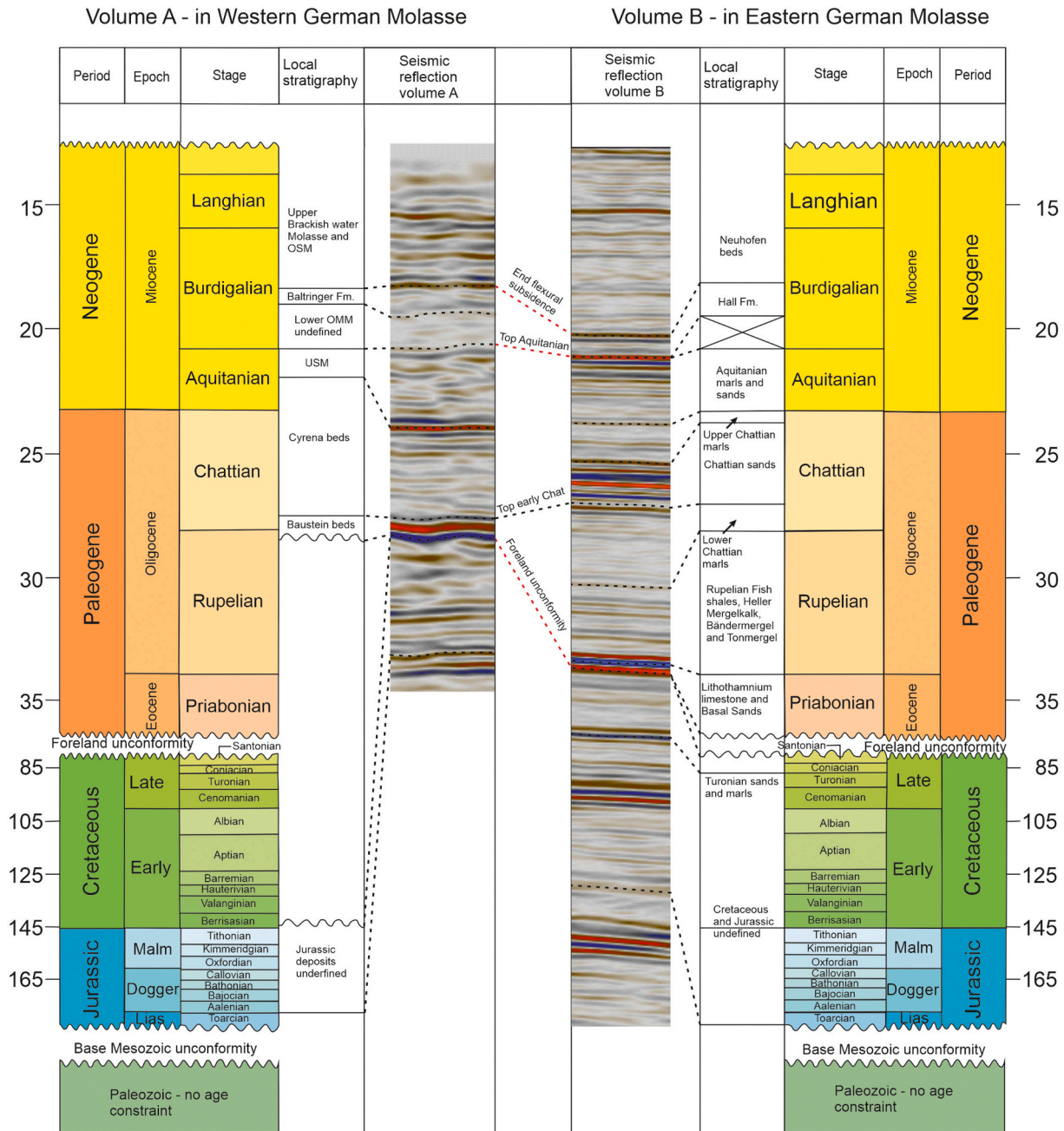


Fig. 2. Stratigraphic column of the western and eastern German Molasse Basin (study area). Reflectors that indicate the same tectonic event or age are connected with red dashed lines. In seismic volume A, the ages of the surfaces are based on (Kuhlemann and Kempf, 2002; von Doppler et al., 2005; Heimann et al., 2009; Heckeberg et al., 2010; Shipilin et al., 2020). Ages from the surfaces in seismic volume B are based on (Jin et al., 1995; Zweigel et al., 1998). The ages of the stratigraphy in the parts of Molasse Basin covered by these seismic volumes are derived from biostratigraphy, which yields 1 to 2 Myrs of uncertainty. The stratigraphic gap in the early Burdigalian is based on the time gap presented by the unconformity at the base of the Hall Formation in the Eastern German Molasse (BHU, Hülscher et al., 2019).

the eastward tectonic escape of the Eastern Alps rather than continued northward migration (Ratschbacher et al., 1991; Rosenberg et al., 2007; Favaro et al., 2015). This tectonic reorganisation was contemporary with the cessation of subsidence in the Eastern Molasse (20 to 18 Ma, Genser et al., 2007; Ortner et al., 2015; Schlunegger and Kissling, 2022). Only southeast of Munich did the subsidence continue after the early Burdigalian (Zweigel et al., 1998). Furthermore, the tectonic reorganisation in the Eastern Alps was coeval with the onset of southward in-sequence thrusting in the Southern Alps (Schönborn, 1999; Caputo et al., 2010).

2.2. Stratigraphy of the foreland plate

The following sections give a synoptic overview of the pre-flexural Mesozoic basement stratigraphy (Subsection 2.2.1) and syn-flexural basin fill of the Molasse Basin (Subsection 2.2.2).

2.2.1. Paleozoic and Mesozoic basement

The Variscan crystalline basement of the MB consists of gneisses and granites (Herrmann et al., 1985; Bachmann and Müller, 1991), locally cut by Carboniferous to Triassic grabens (Bachmann and Müller, 1991; Gautschi et al., 2008). This is overlain by Middle Triassic to Late Cretaceous passive margin sediments with a spatially variable thickness distribution (Frisch, 1979; Nachtmann and Wagner, 1987; Ziegler, 1990; Bachmann and Müller, 1991). From west to east, the Mesozoic subcrop of the foreland unconformity changes from Late Jurassic to Late Cretaceous stratigraphy (Lemcke, 1988; Bachmann and Müller, 1991).

2.2.2. Cenozoic syn-flexural fill of the Molasse Basin

The oldest Cenozoic deposits of the Western Molasse are found in the parautochthonous cover of the Aar Massif (now part of the fold-and-thrust-belt). Here, Infrahelvetian Lutetian (middle Eocene) littoral sands and limestones overlie the foreland unconformity (Allen et al., 1991; Menkveld-Gfeller, 1995; Menkveld-Gfeller, 1997; Sinclair, 1997b). These deposits are covered by turbiditic bathyal middle to late Eocene sediments (Globigerina marls and Taveyannaz Fm., Allen et al., 1991; Sinclair, 1997b; Sissingh, 1997; Burkhard and Sommaruga, 1998). In contrast, similar coeval deposits are either scarce or lacking in the autochthonous Western Molasse (up to 10 m thickness, Lemcke, 1988; Müller, 2011). The littoral platform limestones overlying the foreland unconformity represent the lower unit of the underfilled trinity (*sensu* Sinclair, 1997b), succession of littoral platform limestones overlain by hemipelagic marls and subsequently bathyal siliciclastic turbidites). This unit is interpreted to record a foreland basin's initially slow and sediment-starved subsidence. Early Rupelian bathyal turbiditic conditions are recorded in the entire autochthonous Western Molasse (Elm and Matt Fms. of the parautochthonous cover of the Aar Massif, Deutenhausen Beds, and Rupelian fish Shale for the Western German Molasse, Pfiffner, 1986; Allen et al., 1991; Sissingh, 1997; Maurer, 2006). By the late Rupelian, deposition shallowed to neritic conditions along the southern basin margin (Lower Marine Molasse for the Swiss Molasse and Rupelian Tonmergel/Zupfing Fm. for the Western German Molasse, Diem, 1986; Allen et al., 1991; Sissingh, 1997; Mraz et al., 2018). In the Western Molasse, this shallowing (*i.e.*, the underfill- to overfill transition) occurred between 31.5 and 30 Ma, reaching as far east as the Allgäu (Schlunegger et al., 1997b; Kempf et al., 1999; Kempf and Pross, 2005). The shallowing was contemporaneous with the development of alluvial megafans along the Swiss Alpine front (Honegg-Napf, Rigi, and Speer fan systems, 31–30 Ma, Schlunegger et al., 1996; Kempf et al., 1999). By the late Rupelian, littoral conditions in the Swiss Molasse (Horw Sandstones, Diem, 1986), transitioned into neritic conditions in the Western German Molasse (Rupelian Tonmergel, Zaugg and Löpfle, 2011; Mraz et al., 2018). Littoral depositional conditions reached the Western German Molasse by the earliest Chattian (28 Ma onset of Baustein Beds deposition, Mraz et al., 2018). From the middle Chattian until the end of the Aquitanian, the Western Molasse developed as an

eastward draining fluvial environment (26 to 20.5 Ma, Lower Freshwater Molasse and Cyrena Beds, Matter, 1980; Platt, 1992; Platt and Keller, 1992; Kuhlemann and Kempf, 2002; Reichenbacher et al., 2004; Ziegler and Storch, 2008). Subsequently, this fluvial environment was flooded during the early Burdigalian Transgression, leading to the re-establishment of neritic depositional conditions between 20 and 17 Ma (St. Gallen, Luzern and Baltringer Fms., Matter, 1980; Lemcke, 1988; Keller, 1989; Schlunegger et al., 1997a; Garefalakis and Schlunegger, 2019). However, the depositional environment quickly shallowed back to terrestrial conditions during the middle to late Burdigalian (Matter, 1980; Kuhlemann and Kempf, 2002). Furthermore, the drainage direction switched from the east to the west (Kuhlemann and Kempf, 2002; Garefalakis and Schlunegger, 2019).

In the Eastern Molasse, neritic Lutetian (middle Eocene) strata in the Helvetic nappes of the Eastern Alps were deposited in the Helvetic domain, grading southward into bathyal conditions (Adelholzener Schichten, Schwarzerzschichten, and Flöz-Nebengestein, Heyng, 2012). Subsequently, Priabonian (late Eocene) sediments record a deepening of the entire Helvetic domain to bathyal flysch conditions (Stockletten, Heyng, 2012). This was coeval with littoral deposition on top of the foreland unconformity in the autochthonous Eastern Molasse (Basal Sands and Lithothamnium Limestones, Sissingh, 1997; Wagner, 1998; Zweigel et al., 1998). Early Rupelian (34 to 31 Ma) deposition of bathyal marls and turbiditic sands evidence a subsequent rapid deepening to underfilled flysch conditions (Fish shales/Schöneck Fm. and Heller Mergelkalk/Dynow Fm., Bachmann and Müller, 1991; Jin et al., 1995; Sissingh, 1997; Wagner, 1998; Zweigel et al., 1998). By the late Rupelian (31 to 28 Ma), conditions shallowed from bathyal to neritic following the maximum flooding surface recorded within the Heller Mergelkalk (Bändermergel/Eggerding Fm., Tonmergel/Zupfing Fm., Deutenhausen Fm., Bachmann and Müller, 1991; Jin et al., 1995; Sissingh, 1997; Wagner, 1998; Zweigel et al., 1998; Hülscher et al., 2019). This means the underfilled trinity is prevalent in both the Eastern Alpine nappe stack and the autochthonous Eastern Molasse. Continued shallowing led to the deposition of littoral sands (also considered as underfilled- to overfilled transition) in the Eastern German Molasse by the middle Chattian (26 Ma, Chattian Sands, Jin et al., 1995; Zweigel et al., 1998). However, bathyal conditions remained dominant in the Austrian Molasse throughout the Chattian and Aquitanian (Puchkirchen Fm. recording up to 1000–1500 m water depths, Rögl et al., 1979; Wagner, 1998; De Ruig and Hubbard, 2006; Hülscher et al., 2019). This juxtaposition of under- and overfilled conditions led to the development of the littoral to neritic eastward facing Bavarian Shelf (Jin et al., 1995; Zweigel et al., 1998). To the south, the Austrian Molasse was flanked by fluvio-deltaic wedge-top deposition (Augenstein Fm. on top of the future Northern Calcareous Alps and Inneralpine Molasse in the Lower Inn Valley, Frisch et al., 2001; Ortner and Stingl, 2001; Sharman et al., 2018; Hülscher et al., 2019). Apart from a short period of drowning during the late Chattian (24 Ma), the Bavarian shelf remained at a relatively stationary position during the late Oligocene to early Miocene (Lemcke, 1988; Jin et al., 1995; Zweigel et al., 1998). Like the Western Molasse, the early Burdigalian Transgression led to a re-establishment of neritic conditions in the Eastern German Molasse (Obing Fm., Lemcke, 1988; Jin et al., 1995; Zweigel et al., 1998) while bathyal deposition remained dominant in the Austrian Molasse (basal Hall Fm. overlying Base Hall Unconformity (BHU), De Ruig and Hubbard, 2006; Hülscher et al., 2019). However, by the middle to late Burdigalian (18 to 17 Ma), terrestrial and neritic deposition was dominant in the Eastern German and Austrian Molasse, respectively (Upper Freshwater Molasse, Neuhofen Beds and Upper Hall Fm., Jin et al., 1995; Zweigel et al., 1998; De Ruig and Hubbard, 2006; Hülscher et al., 2019). This evidences a rapid transition from underfilled- to overfilled conditions in the Eastern Molasse at 19–18 Ma (Hülscher et al., 2019).

3. Data and methods

We constructed a 3D geological model from present-day sea level to 8000 m depth to determine the influence of the European passive margin architecture on MB evolution (Subsection 3.1). In addition, 2D/3D reflection seismic data as interpreted using the Petrel software* to reconstruct the tectonostratigraphic evolution of the MB. These results are then compared with the tectonic evolution of the adjacent Alps to find spatiotemporal relationships between orogenic processes and basin response (Subsection 3.2).

3.1. Depth grids and construction of 3D geological model

The 3D geological model of the MB was generated using the 2015 GeoMol subsurface models (GeoMol, 2015) of the Swiss, German, and Austrian Molasse (Fig. 1a for locations). The subsurface models are based on seismic interpretations, borehole data, and models from previous studies (GeoMol, 2015). The stratigraphic surfaces used in each part of the model are given in Table 1. The structural modelling tool in Petrel* was used to combine the datasets to generate surfaces spanning the entire MB. This tool uses a volume-based implicit approach (see Mallet, 2004; Caumon and Mallet, 2006) to create a stratigraphic function based on the type of horizon (conformable, erosional, base, or discontinuous) and input surfaces. In interpolated areas, thickness trends from data-covered regions are preserved. Surfaces were generated for the top crystalline basement, top Lower Jurassic, top Middle Jurassic, top Upper Jurassic, base Lower Marine Molasse (UMM), base Lower Freshwater Molasse (USM), base Upper Marine Molasse (OMM) and base Upper Freshwater Molasse (OSM) (*sensu* Matter, 1980). Eocene deposits are incorporated in the UMM deposits because of their minor thickness relative to the size of the model. For generated thickness maps, areas with <50 m thickness are removed to highlight areas of significant deposition during the respective time windows. The geological model does not extend below the thrust front, as the confidence of the input data is lower there. Subsequently we generated thickness distribution maps for the Middle Jurassic, Upper Jurassic, and Cretaceous using the model results. The thickness distributions provide insights into the paleogeography of the European shelf during the Jurassic and Cretaceous and the basin floor architecture at the onset of flexural subsidence.

3.2. Seismic data

Seismic volumes A and B cover parts of the Western- and Eastern German Molasse, respectively (Fig. 1a for locations). Seismic volume A

is an APSDM cube (anisotropic pre-stack depth migrated) in the depth domain and covers an area of 145 km², imaging to depths of up to 2000 m. Seismic volume B is a PreSTM (pre-stack time migrated) cube in the time domain located on the Bavarian Shelf, covering an area of 560 km². The upper 2500 ms TWTT of this volume was of sufficient quality to interpret. Both volumes are displayed in reverse polarity (SEG convention). This means that a downward increase in acoustic impedance is represented by a trough (Fig. 2; blue reflectors with negative amplitudes) and a decrease in acoustic impedance is reflected by a peak (Fig. 2; red reflectors with positive amplitudes). The seismic volumes are separated by a 100 km-wide gap covered by sparse 2D seismic data (Fig. 1a, Großmann et al., 2024). The structural smoothing attribute was applied to the input seismic data for conventional horizon tracing to increase the signal/noise ratio. Important stratigraphic surfaces and unconformities are identified for each seismic volume using borehole data. Eight different reflectors are mapped in seismic volume A, which are from top to bottom: Top Baltringer Fm., top USM, top Cyrena Beds, top Baustein Beds, top Malm, base karstified Malm, top Dogger and top Lias (Fig. 2). Eight seismic horizons were also mapped in seismic volume B, which are from top to bottom: top Hall Fm., Base Hall Unconformity (BHU, *sensu* De Ruig and Hubbard, 2006; Hülscher et al., 2019), top Chattian Sands, top Rupelian, top Eocene, base Eocene, top Turonian and base Mesozoic (Fig. 2). Faults cross-cutting the seismic-stratigraphic units were interpreted based on lateral reflector terminations. To enhance the confidence of the fault interpretation, the variance seismic attribute was applied to the input seismics (Subrahmanyam and Rao, 2008; Koson et al., 2013).

Active frontal thrusting drove the migration of the flexural forebulge around which the syn-flexural normal faults were active, thereby governing the spatiotemporal location of the zone of extensional stresses (DeCelles and Giles, 1996; Supak et al., 2006; Langhi et al., 2011; DeCelles, 2012). As the forebulge migrated further cratonward, normal faults cut progressively younger stratigraphy. Therefore, normal faults further from the present-day thrust front cut younger stratigraphy compared to their counterparts closer to the thrust front (Fig. 3a). The spatiotemporal syn-flexural normal fault activity derived from growth strata (Fig. 3b) enabled inference of high and low intensities in frontal thrusting activity (Bry et al., 2004). This allowed reconstruction of spatiotemporal variations in hinterland tectonics from syn-flexural normal fault activity in the foreland basin. Furthermore, differences in cumulative Cenozoic offsets along the syn-flexural normal faults implicate a higher magnitude of flexural bending of the European plate. This may have resulted from variations in either 1) combined topographic- and slab loading (Flemings and Jordan, 1990; Sinclair, 1997a) and/or 2)

Table 1

Available surfaces in the various parts of the 2015 GeoMol model. Undefined stands for a lack of definition of whether the top of the Cretaceous consists of Lower, Middle, or Upper Cretaceous sediments. A dash implies a dataset does not contain the respective base or top.

Units/Data source	Swiss Molasse Basin 2015 GeoMol	Western German Molasse Basin 2015 GeoMol	Eastern German Molasse Basin 2015 GeoMol	Austrian Molasse Basin 2015 GeoMol
Crystalline basement		Top	Top	Top
Permo-carboniferous	Base	–	–	–
Lower Triassic	Base	–	–	–
Middle Triassic	Top	–	–	–
Upper Triassic	Top	–	–	–
Lower Jurassic	Top	Top	–	–
Middle Jurassic	Top	Top	–	Base
Upper Jurassic	Top	Top	Base	Base
Lower Cretaceous	–	–	–	–
Middle Cretaceous	–	–	–	–
Upper Cretaceous	Top (undefined)	Top (undefined)	Base (undefined)	Base
Late Eocene	Base	–	Base	Base
Lower Marine Molasse	Top	Base	Base	Base
Lower Freshwater Molasse	Top	Base	Base	Base
Upper Marine Molasse	Top	Base	Base	Base
Upper Freshwater Molasse	–	Base	Base	Base

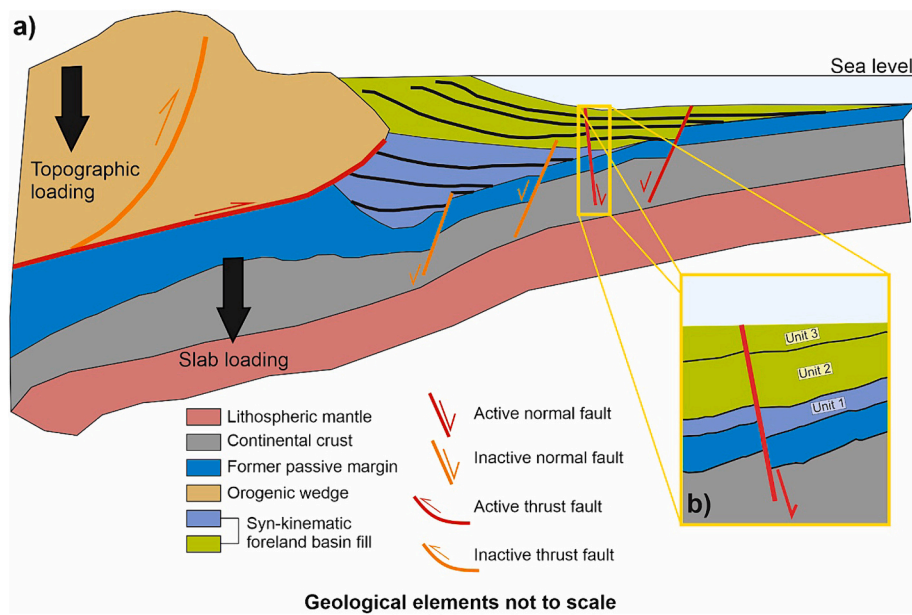


Fig. 3. a) Schematic illustration of normal faults cutting the crystalline basement, pre-flexural passive margin sediments, and syn-flexural fill of a foreland basin. Generally, normal faults located further away from the present-day thrust front are expected to cut younger syn-flexural fill compared to normal faults closer to the thrust front. This is due to the cratonward migration of the flexural forebulge (*i.e.*, extensional stress field) as the thrust front propagates further onto the foreland plate. b) Schematic zoom-in showing how stratigraphic thickness changes caused by syn-flexural normal faulting can be used to infer the spatiotemporal activity of normal faults. Syn-flexural units 1 and 3 record thickness changes across the fault, whereas unit 2 does not record changes across the fault. This alternation in activity and inactivity of the normal faults in foreland basins can be used to infer periods where and when extensional stresses due to flexural subsidence were (not) affecting the foreland plate at the location of the seismic data.

strength variations of the European plate (Flemings and Jordan, 1989; Waschbusch and Royden, 1992).

With this concept in mind, we apply the “original” backstripping method (Chapman and Meneilly, 1991; Petersen et al., 1992). Alternative methods, such as the “modified” backstripping method (Rowan et al., 1998), could also be applied. However, the latter method assumes that a normal fault grows laterally according to the isolated fault model (*e.g.*, Cartwright et al., 1996; Mansfield and Cartwright, 1996). Because of this assumption, we chose not to use this method. For the “original” backstripping method, throws of successively deeper interpreted reflectors at the same position along the strike of a normal fault are subtracted from each other. This subtraction results in the syn-kinematic thickening of a seismic-stratigraphic unit between two different reflectors across a normal fault. This can be plotted as a backstripped throw-length (T-x) profile showing spatiotemporal variations in the slip rate along a fault and lateral growth styles of normal faults (*e.g.*, Jackson et al., 2017; Robson et al., 2017; Tvedt et al., 2013). Backstripped T-x profiles of the two faults that record the highest cumulative Cenozoic offset in each seismic volume (thought to reflect best the structural style in the respective parts of the German Molasse) are presented. Spatiotemporal development of the depositional environment in the German Molasse based on our seismic interpretations are compared to the spatiotemporal variations in flexural subsidence inferred from the T-x profiles to verify our results.

4. Results

First, we present the 3D geological model of the thickness distributions of the different Mesozoic basement units and an orogen-parallel profile through the MB (Subsection 4.1). This is followed by the seismic data in both volumes to constrain the tectonostratigraphic evolution in different parts of the German Molasse (Subsection 4.2). Finally, syn-flexural normal fault kinematics are quantified to assess

along-strike variations in the timing and magnitude of flexural subsidence in the German Molasse (Subsection 4.3).

4.1. 3D basin model of the entire Molasse Basin

The Mesozoic units start with the Middle Jurassic deposits, whose thickness decreases from ~450 m in the western Swiss Molasse to <100 m in the German Molasse (Fig. 4a). The overlying Upper Jurassic reaches its highest thicknesses at the western (up to 1100 m, western Swiss Molasse) and eastern (~700 m south of Munich) basin margins, from which it thins to 250 m around Zürich (Fig. 4b). The Cretaceous stratigraphy is thickest southeast of Munich (~900 m), whereas in the other parts of the basin it is either absent or the thickness is <100 m (Fig. 4c).

In the orogen-parallel direction, the top of the crystalline basement dips 0.3° eastwards from the Swiss- to German Molasse (between 100 and 480 km in Fig. 5, for the location of the orogen-parallel cross-section, see Figs. 1a and 4). The crystalline basement in the Swiss- and German Molasse is locally cut by Permo-Carboniferous grabens, also imaged in our 3D seismic dataset (see Subsection 4.2, Figs. 5, 7, and A2). In the Austrian Molasse, the top of the crystalline basement has a westward tilt (around 500 km; Fig. 5). This likely represents the Central Swell (also observed by Ortner et al., 2023; their Fig. 5.2). Triassic to Middle Jurassic deposits in the eastern Swiss- and Western German Molasse thin from both the west- and east onto the crystalline basement located at a shallow depth around Zürich (between 100 and 300 km, Fig. 5). Between Zürich and the Bavarian Shelf, Upper Jurassic, and Cretaceous successions thicken to the east from ~700 to ~1600 m (Fig. 5).

4.2. Seismic stratigraphy of seismic volumes A and B

4.2.1. Mesozoic basement units

In seismic volume A, the base of the seismically interpretable

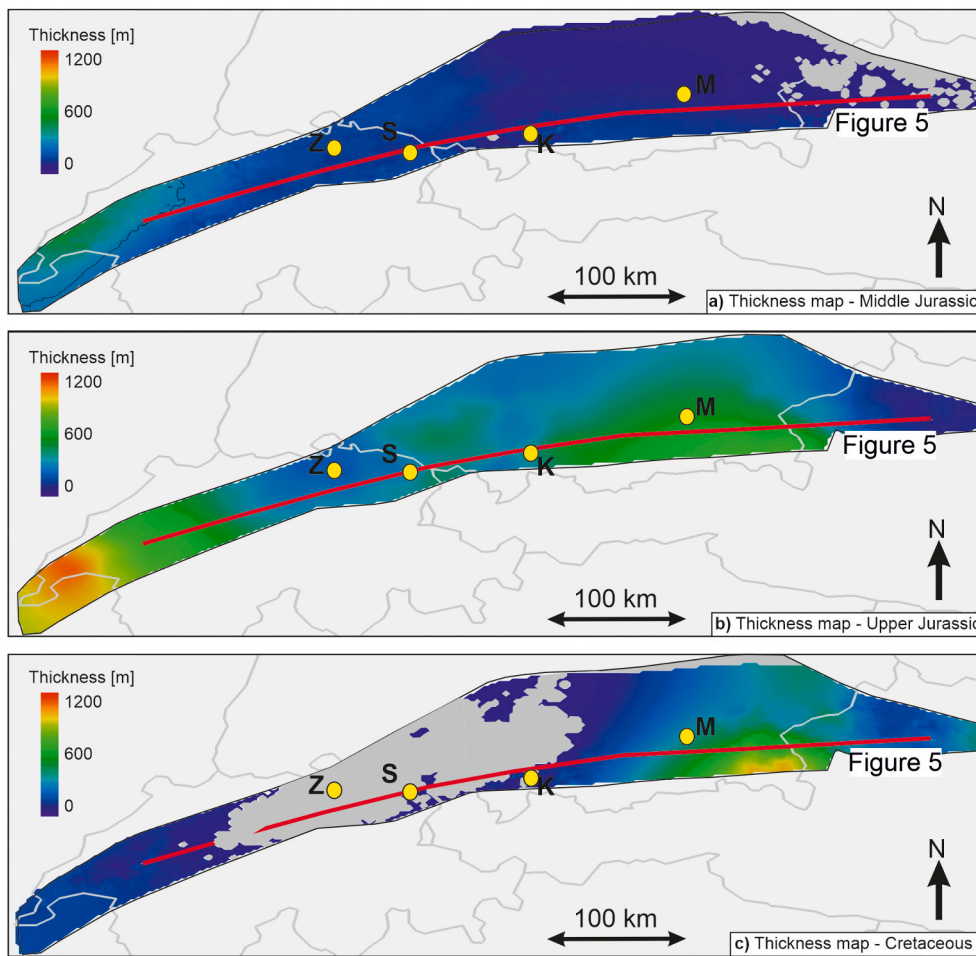


Fig. 4. Thickness distribution of the a) Middle Jurassic, b) Upper Jurassic, and c) Cretaceous deposits in the Molasse Basin resultant from the 3D model. Grey areas indicate where the thickness of the respective deposit is below 50 m and are not shown because this is below model resolution. K = Kaufbeuren, M = Munich, S = St. Gallen, Z = Zürich.

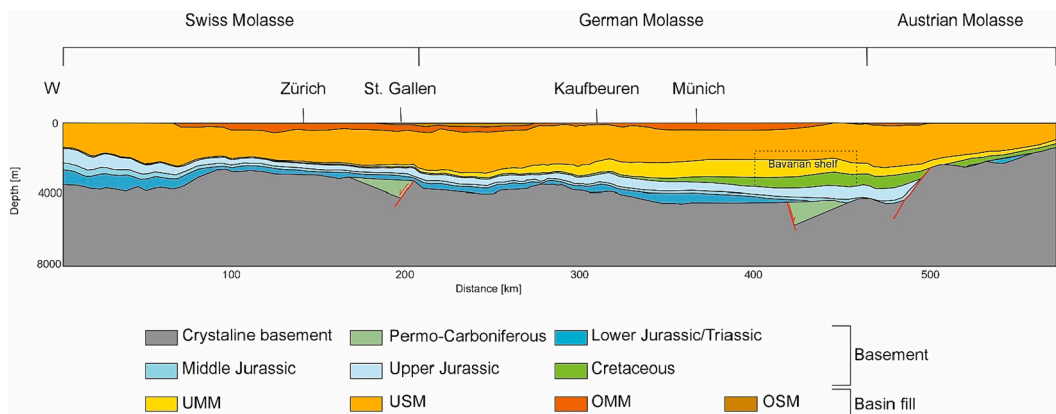


Fig. 5. Along-strike profile through 3D geological model (for exact location see Fig. 1a). The position of the Permo-Carboniferous graben in Swiss Molasse is based on previous studies (Bachmann and Müller, 1991; Heuberger et al., 2016). Black dashed boxes give the locations of the Bavarian Shelf Eastern German Molasse. Apart from faults bounding Paleozoic graben structures in the Swiss Molasse and west of the Central Swell (Ortner et al., 2023), normal faults are not drawn in this section as they were not explicitly modelled as they have relatively small offsets for our model.

Mesozoic sequence is defined by the top Lower Jurassic (Lias) reflector (Fig. 6). The overlying Middle Jurassic unit is characterised by SF-A1 (Table 2, Fig. 6). The Upper Jurassic unit concordantly overlies the Middle Jurassic and is characterised by an internal stratigraphically upward transition from SF-A1 to SF-A2 (Table 2, Fig. 6). This reflects a

shift from non-karstified to karstified limestones (also observed in borehole data, Lemcke, 1988; Meyer and Schmidt-Kaler, 1990). The distribution of amplitudes of the variance attribute of the Upper Jurassic unit (Fig. A3) indicates a high degree of karstification in the WNW, whereas in the ESE there is little- to no karstification. The top of the

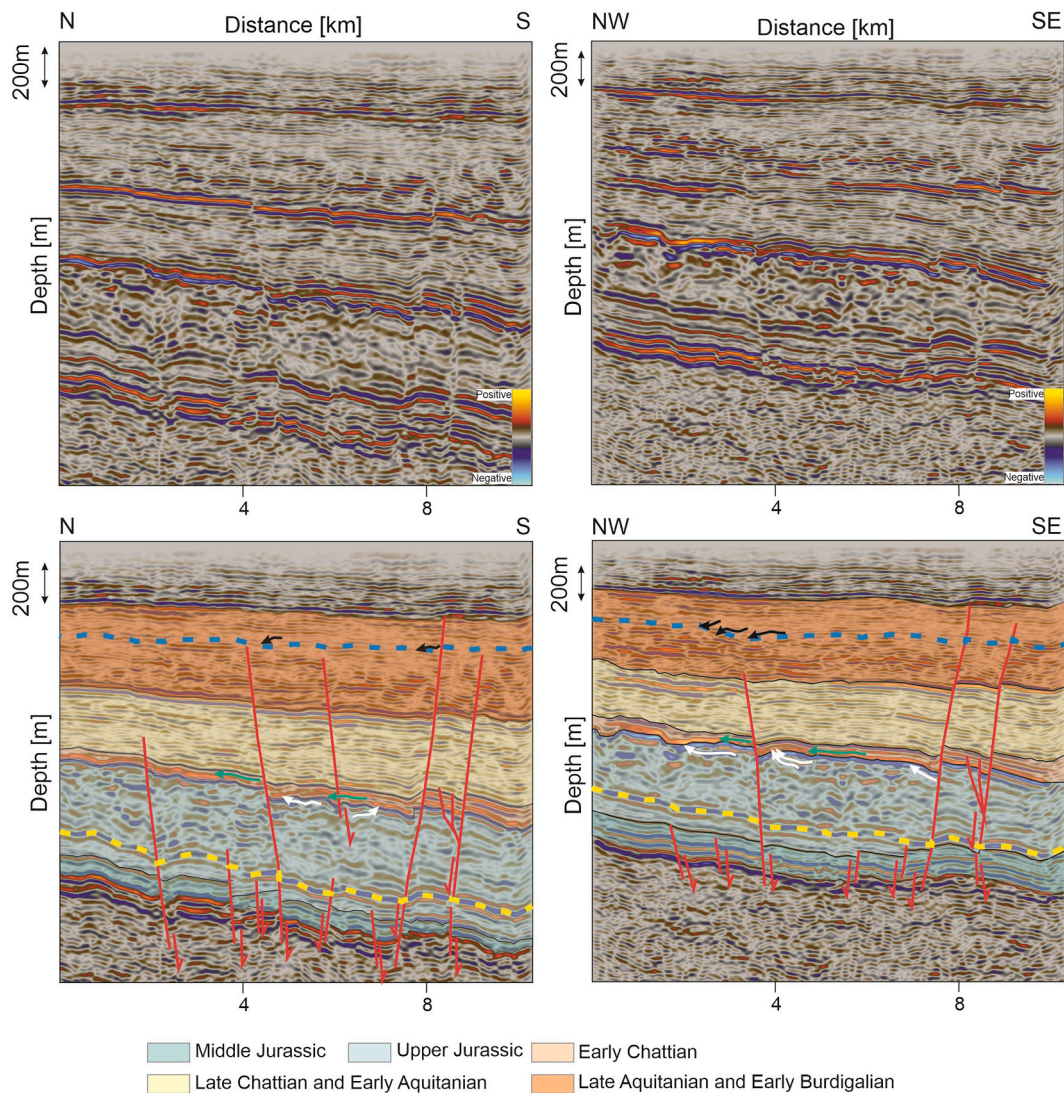


Fig. 6. The upper panels show uninterpreted examples of N-S and NW-SE seismic lines through seismic volume A. The bottom panels show the same lines with the seismic-stratigraphic bodies interpreted throughout the entire seismic volume. Red lines indicate normal faults and their respective kinematics, the yellow dashed reflectors marks the base of the karstified Upper Jurassic sequence, and the blue dashed line is the top Aquitanian reflector. White arrows mark terminating Upper Jurassic reflectors against the top Upper Jurassic, green arrows terminating early Chattian reflectors against the top Upper Jurassic, and black arrows terminating early Burdigalian reflectors against the top Aquitanian.

Jurassic is defined by a strong negative amplitude reflector against which both Upper Jurassic and late Chattian reflectors terminate (Fig. 6; white and green arrows). This characterises the foreland unconformity in seismic volume A.

The Mesozoic sequence in seismic volume B consists of Jurassic and Cretaceous deposits, locally underlain by the Paleozoic-Triassic Giftthal Through (Figs. 7 and A1, Bachmann and Müller, 1991). The Mesozoic sequence below the top Turonian reflector does not show thickness changes across the normal faults that cut the syn-flexural Cenozoic stratigraphy (Fig. 7). The post-Turonian Late Cretaceous unit is characterised by SF-B1, which concordantly overlies the undefined portion of the Mesozoic sequence (Fig. 7). This unit records an eastward-directed thickening from 10 to over 250 m, unrelated to the syn-flexural normal faults (Fig. A4). Post-Turonian reflectors terminate against the Base Eocene (Fig. 7; white arrows), marking the foreland unconformity in seismic volume B.

4.2.2. Late Eocene - Priabonian

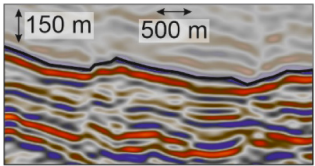
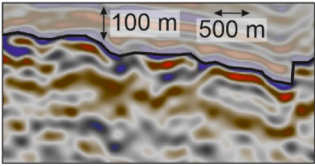
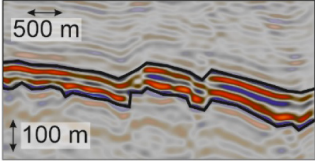
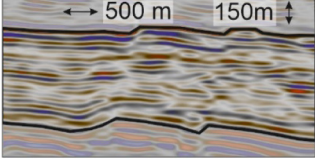
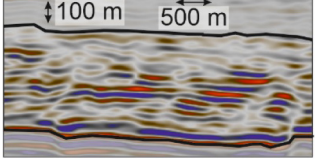
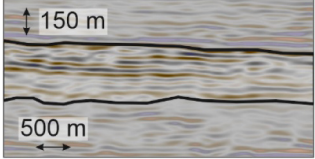
Late Eocene deposits are absent in seismic volume A. In contrast,

they are represented in seismic volume B by SF-B2 (Fig. 7, Table 2), and interpreted as the Priabonian (Late Eocene) Basal Sands and Lithothamnium Limestones (well data; Sissingh, 1997; Wagner, 1998; Zweigel et al., 1998). These deposits overlie the foreland unconformity and dip to the south (Fig. 7). At the top, they are conformably overlain by SF-B3 (Fig. 7, Table 3).

4.2.3. Early Oligocene – Rupelian

Rupelian deposits are absent in seismic volume A. In seismic volume B, the top of the Eocene is marked by a prominent negative amplitude reflector (Fig. 7). Based on well data and previous studies (Jin et al., 1995; Zweigel et al., 1998), the overlying SF-B3 is interpreted as Rupelian bathyal to neritic marls and sands. This unit shows a west-to-east thinning from 350 m to 100 m (Fig. A5). Strikingly, this is the opposite of what is observed for the thickness distribution of the post-Turonian Mesozoic unit (Subsection 4.2.1). Southward thickening towards syn-flexural normal faults (Fig. A5) reveals the syn-kinematic nature of these sediments. While the lower part of the Rupelian succession is defined by a homogeneous distribution of SF-B3 in the entire

Table 2
Seismic facies (SF) examples, descriptions, and interpretations of seismic volume A.

Seismic facies	Example	Description	Interpretation
SF-A1		High frequency, high to medium amplitude reflections with good lateral continuity	Alternation of marine limestones and marls.
SF-A2		Low frequency, high to low amplitude reflections with poor lateral continuity. Overall chaotic seismic facies	Heavily karstified platform limestones.
SF-A3		High frequency, high to medium amplitude reflections with good lateral continuity.	Littoral sands containing cross beds
SF-A4		High frequency, low to medium amplitude reflections. Semi-continuous reflectors showing overall semi-chaotic seismic facies	Heterolithic brackish deposits, transition between littoral and terrestrial depositional environments
SF-A5		High frequency, low to high amplitude reflections with very poor lateral continuity. Overall chaotic seismic facies	Littoral to terrestrial deposits; meandering channels and overbank deposits, and lakes
SF-A6		Low frequency, low to medium amplitude reflections with medium to good lateral continuity. Upward in the facies the amplitude and lateral continuity increase	Neritic deposits consisting of a mix of sands and shales

volume, it grades stratigraphically upward to SF-B4 to the NW (Fig. 7, Table 3). This means that while the NW bathyal conditions graded into neritic and littoral deposition, bathyal conditions remained dominant in the SE throughout the Rupelian. The top of the Rupelian seismic stratigraphy is characterised by a low negative amplitude reflector, cutting down into both SF-B3 and SF-B4 of the Rupelian unit (yellow arrows in Fig. 7, Fig. A6). Early Chattian reflectors onlap onto the top Rupelian towards the NW (Fig. 7; yellow arrows).

4.2.4. Late Oligocene – Chattian

The oldest Cenozoic deposits preserved in seismic volume A are the early Chattian Baustein Beds (based on well data). This unit is characterised by SF-A3 (Table 3) with reflectors at the base onlapping to the NNW onto the foreland unconformity (green arrows in Fig. 7). The observed patches of increased thicknesses of the early Chattian deposits (Fig. A7) suggest infilling of Upper Jurassic karst pockets. The sweetness attribute map of the early Chattian unit (Fig. A8) shows N-S striking bands of high values in the west, with the SE characterised by low values. This implies the development of an N-S striking coastline with sand-rich deposits in the west, grading into more shale-rich deposits in

the east. Well data shows that the early Chattian stratigraphy contains cross-beds and is cemented at the top by freshwater, fossil-rich carbonates, and coaly silts and marls. This suggests that the early Chattian deposition in seismic volume A are characterised by littoral deposition grading upward into freshwater conditions.

The concordantly overlying seismic-stratigraphic unit represents the middle to late Chattian Cyrena Beds (based on well data). This unit is characterised by a shift to SF-A4 (Fig. 7, Table 2). Thickness changes up to 100 m towards the syn-flexural normal faults (Fig. A9) reveal the syn-kinematic nature of this unit. A variance slice through this unit (Fig. A10) reveals the presence of meandering channels, suggesting freshwater conditions at the end of the early Chattian continued to develop into delta plain and fluvial conditions.

The early Chattian reflectors overlying the Rupelian unit in seismic volume B characterise the Lower Chattian Marls (well data, Jin et al., 1995; Zweigel et al., 1998). The seismic facies of this unit (SF-B4, Table 3) are similar to that of the underlying Rupelian in the WNW of the data volume, with clinoforms migrating to the ESE across the Bavarian Shelf (Fig. 7). Clinoforms are absent in the ESE of the volume for this unit, and SF-B3 remains dominant in the lower Chattian (Fig. 7).

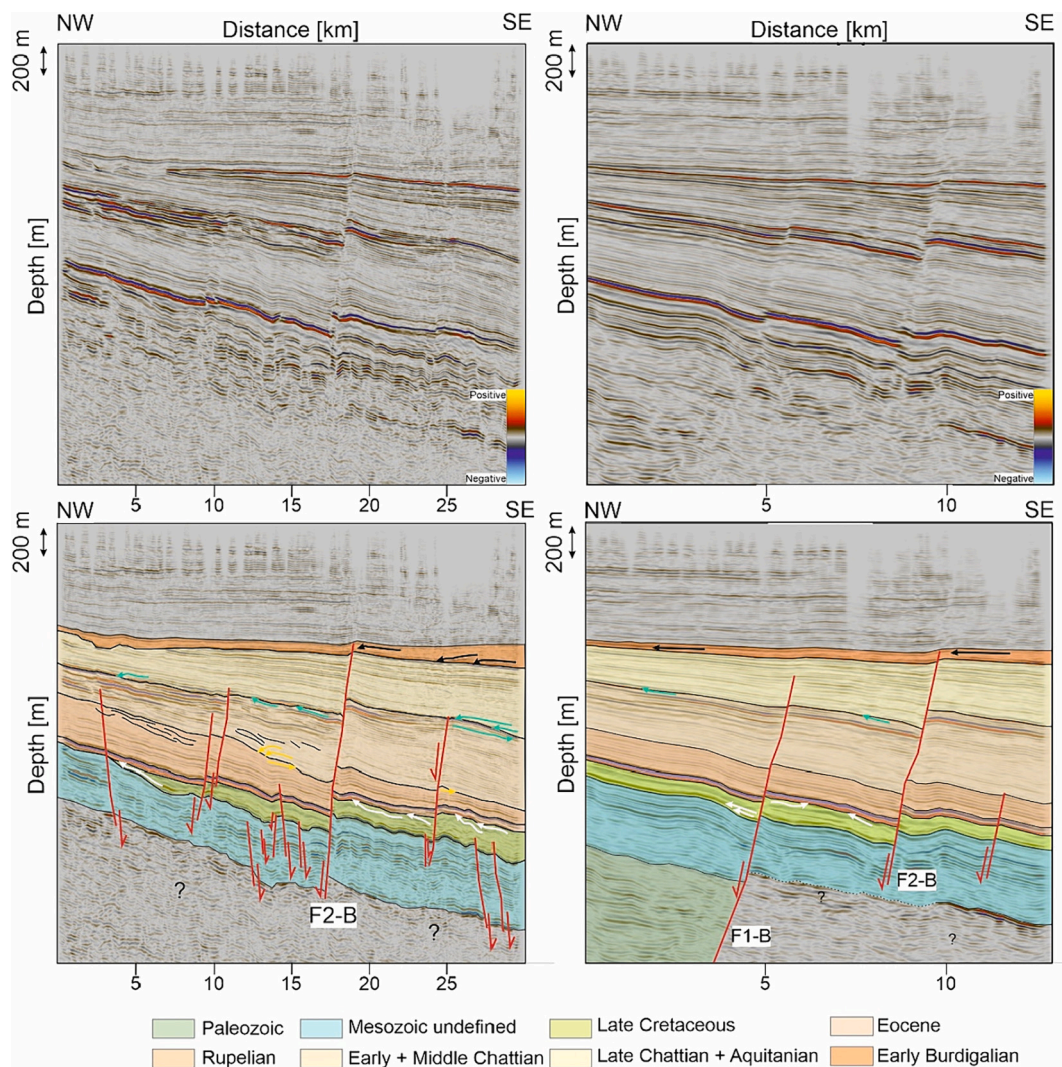


Fig. 7. The upper panels show uninterpreted examples of N-S and NW-SE seismic lines through seismic volume B. The bottom panels show the same lines with the seismic-stratigraphic bodies interpreted throughout the entire seismic volume. Red lines indicate normal faults and their respective kinematics. White arrows mark terminating late Cretaceous reflectors against the Base Eocene, yellow arrows late Rupelian and early Chattian reflector terminations against the top Rupelian, green arrows terminating Middle and early Chattian reflectors against the top Chattian Sands, and black arrows terminating early Burdigalian reflectors against the Base Hall Unconformity.

Stratigraphically upward this is followed by middle Chattian littoral Chattian Sands (well data; Jin et al., 1995; Zweigel et al., 1998) characterised by SF-B5 (Table 3) in the WNW of seismic volume B (Fig. 7). In contrast, the middle Chattian reflectors in the ESE of seismic volume B are characterised by SF-B3 (Fig. 7, Table 3). The sweetness attribute map of the middle Chattian unit (Fig. A11) reveals NE-SW striking bands of high values in the west of the seismic volume and low values in the east. These observations suggest a NE-SW striking coastline grading eastward from littoral/neritic to bathyal conditions.

Middle Chattian reflectors terminate against the top Chattian Sands reflector in the WNW (Fig. 7, green arrows). To the ESE incision into the middle Chattian stratigraphy is observed (Fig. 7; green arrows). The overlying late Chattian unit is characterised by SF-B6 (Fig. 7, Table 3) and represents the neritic Upper Chattian Marls (well data; Jin et al., 1995; Zweigel et al., 1998). Reflectors of this late Chattian unit onlap towards the NNW onto the top Chattian Sands reflector (Fig. 7; green arrows).

4.2.5. Early Miocene – Aquitanian

Early Aquitanian seismic stratigraphy in volume A has the same seismic facies as the underlying Cyrena Beds (Fig. 6, Subsection 4.2.4).

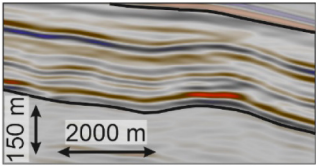
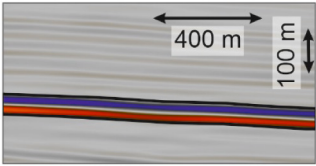
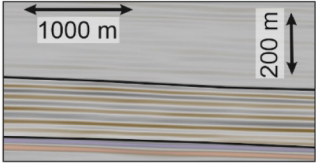
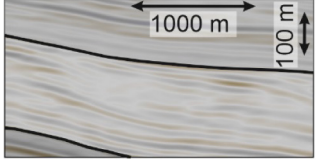
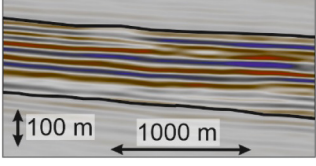
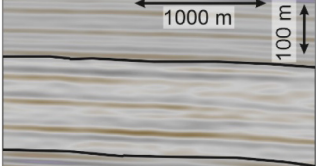
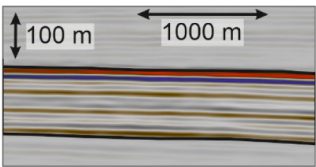
This likely represents an upward continuation of the same depositional environment. The early to late Aquitanian seismic facies grades upward from SF-A4 to SF-A5 (Fig. 6, Table 2). A variance attribute map of the late Aquitanian reflectors (Fig. A12) reveals the continued development of meandering channels.

In seismic volume B, the Aquitanian unit concordantly overlies the Chattian seismic-stratigraphy (Fig. 7) and represents the bathyal- to neritic Aquitanian Series (well data; Jin et al., 1995; Zweigel et al., 1998). In the WNW of the seismic volume, a transition from SF-B4 to SF-B5 is observed at the Chattian-Aquitanian interface (Fig. 7, Table 3). In contrast, in the ESE of the seismic volume, this same change in seismic facies is observed within the Aquitanian unit (Fig. 7). The top of the Aquitanian unit is defined by the BHU against which Aquitanian reflectors tolap (Fig. 7). An incision of Aquitanian deposits is observed in the SE of seismic volume B (Fig. A13, yellow arrows).

4.2.6. Early Miocene – early Burdigalian

The early Burdigalian reflectors in seismic volume A represent an undefined part of the neritic OMM and the Baltringer Fm. (based on well data). Reflectors of this unit onlap towards the NW onto the Aquitanian reflectors (Fig. 6; black arrows). This unit is characterised by SF-A6

Table 3
Seismic facies (SF) examples, descriptions, and interpretations of seismic volume B.

Seismic facies	Example	Description	Interpretation
SF-B1		Medium frequency, high to medium amplitude reflections with good lateral continuity. Lower reflectors are parallel with the upper set showing contrasting dips	A mix of marine shales and sands. The lack of sedimentary structures suggests neritic to bathyal environment
SF-B2		Low frequency, high amplitude pair of parallel reflectors with good continuity	Littoral sands and limestones
SF-B3		Low frequency, medium to high amplitude reflections with good lateral continuity. Reflectors are parallel	Homogeneous bathyal flysch deposits mostly consisting out of shales
SF-B4		High frequency, low to medium amplitude reflections with sigmoidal shapes. Reflectors show internal onlap, downlap and toplap	Clinofolds prograding basinward. Bathyal to neritic transition at the base, neritic to littoral transition closer to the top
SF-B5		High frequency, high to medium amplitude reflections which have varying lateral continuity. Reflectors show internal onlap, downlap and toplap	Littoral deposits consisting out of a mix of sands and shales. Channel geometries towards the top indicate shallowing towards terrestrial conditions
SF-B6		Low frequency, low amplitude reflections with good lateral continuity. Reflectors are subparallel	Neritic deposits consisting mostly out of shales
SF-B7		High frequency, high amplitude reflections with good lateral continuity. Reflectors are subparallel	High frequency, high amplitude reflections with good lateral continuity. Reflectors are subparallel

(Table 2), and the reflectors generally have a shallower southward dip compared to Aquitanian and older reflectors (Fig. 6).

The Aquitanian-Burdigalian transition in seismic volume B is defined by the BHU throughout the entire seismic volume, marking a change from SF-B5 to SF-B4 (Fig. 7). Early Burdigalian reflectors onlap onto the BHU towards the NW and have a shallower SE-directed dip compared to underlying reflectors (Fig. 7; black arrows, Fig. A13; orange arrows).

4.3. Magnitude and timing of syn-sedimentary flexural normal fault activity

Quantifying throw distributions of different reflectors along syn-

flexural normal faults constrains the timing and magnitude of flexural subsidence of the European plate (Fig. 3). In both seismic volumes, syn-flexural normal faults strike E-W (Fig. 8). The exception is F1-B striking NW-SE (Fig. 8). F1-B is a reactivated pre-flexural fault associated with the Permo-Triassic Gifthal Trough (Subsection 4.2.1) leading to its deviating strike. In volume A, syn-flexural faults dipping both to the north and south resulted in the formation of a graben-like structure (Figs. 6 and 8a). In seismic volume B, most faults dip northward (Fig. 8b). The syn-flexural normal faults cut the Mesozoic basement units. Structural maps of early Chattian and early Burdigalian reflectors reveal a reduction in the number of active faults for younger stratigraphy in both seismic volumes (Fig. 8). This implies that as flexure

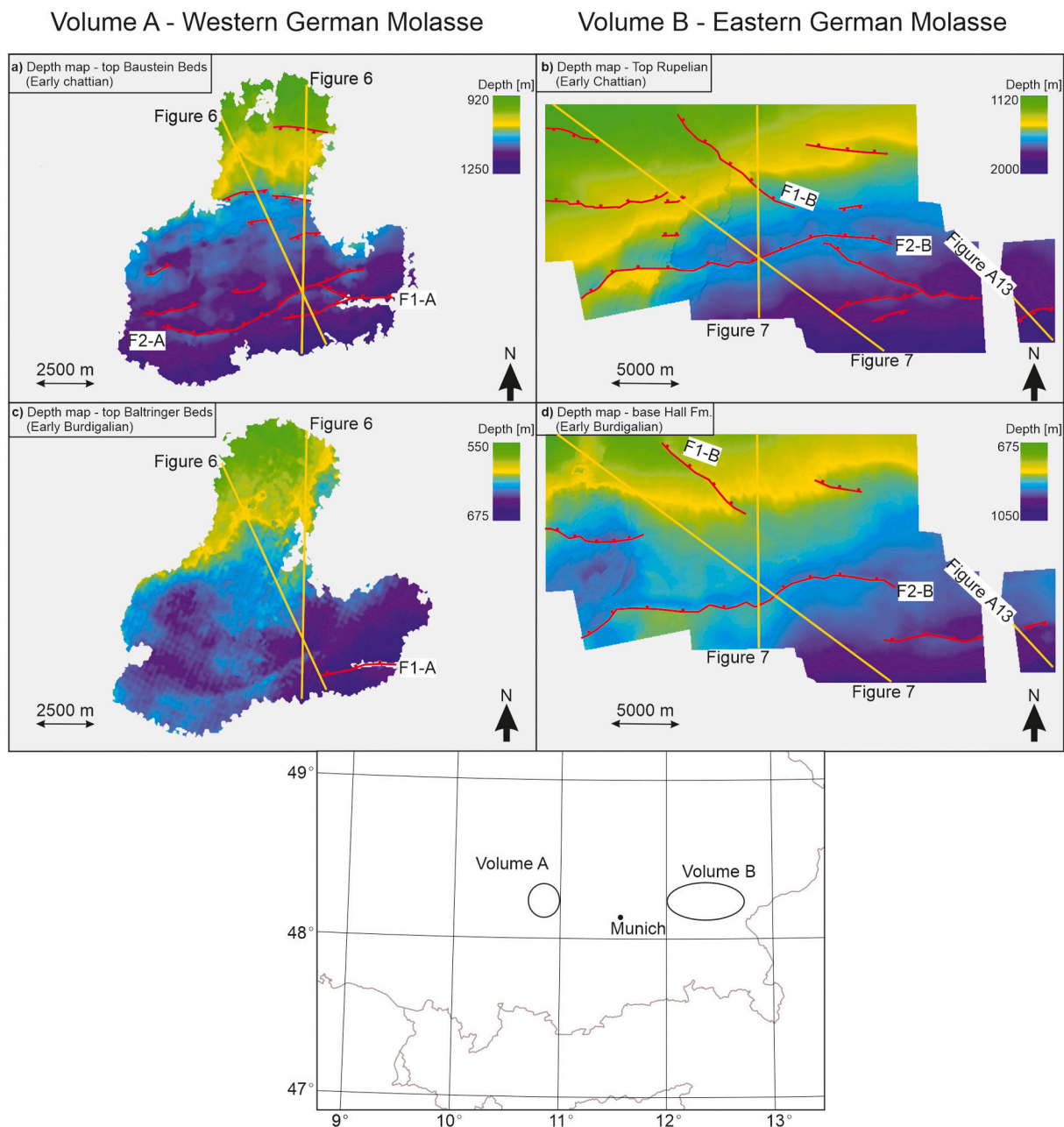


Fig. 8. Depth-structure maps showing the present-day distribution of the normal faults and their dip direction (red lines with blocks indicating the dip direction) in seismic volumes A and B. Surfaces of reflectors of approximately the same age are placed next to each other. The figure below gives the approximate locations of seismic volumes A and B. **a)** top Baustein Beds (*i.e.*, Early Chattian) **b)** top Rupelian Marls and Sands (*i.e.*, early Chattian) **c)** top Baltringer Fm. (*i.e.*, early Burdigalian) **d)** Base Hall Formation (*i.e.*, early Burdigalian). Yellow lines indicate the locations of cross sections shown in Figs. 6, 7, and A13.

continued, the deformation became localised.

The backstripped T-x profile of F1-A shows that fault activity was initiated during the early Chattian in seismic volume A (Fig. 9a). In contrast, in seismic volume B, normal fault activity was initiated in the late Eocene to Rupelian (F2-B, Fig. 9b). During the early to middle Chattian fault activity decreased in seismic volume B (Fig. 9b). However, north of seismic volume B, early to middle Chattian stratigraphy records thickness changes across syn-flexural normal faults (Fig. A14). This suggests a northward migration of the extensional stress field in the Eastern German Molasse. The syn-flexural faults remained active in both study areas until the early Burdigalian (Fig. 9). Comparing the backstripped T-x profiles of faults in seismic volumes A and B shows that fault F1-A records a lower cumulative Cenozoic offset (150 m; Fig. 9a)

compared to F2-B (220 m; Fig. 9b). Furthermore, whereas the longest fault in seismic volume is 8400 m long (Fig. 8a; F2-A), the longest fault in seismic volume B is 25.000 m long (Fig. 8b; F2-B). This implies that the magnitude of syn-flexural normal faulting in volume B exceeded that of volume A.

5. Discussion

Results from the 3D geological model (Figs. 4 and 5) constrain the pre-flexural architecture of the European margin from the Middle Jurassic until the late Eocene onset of flexure. Furthermore, interpreted 3D seismic data (Figs. 6 to 9) highlight late Eocene to early Miocene spatiotemporal variations in depositional environments and syn-flexural

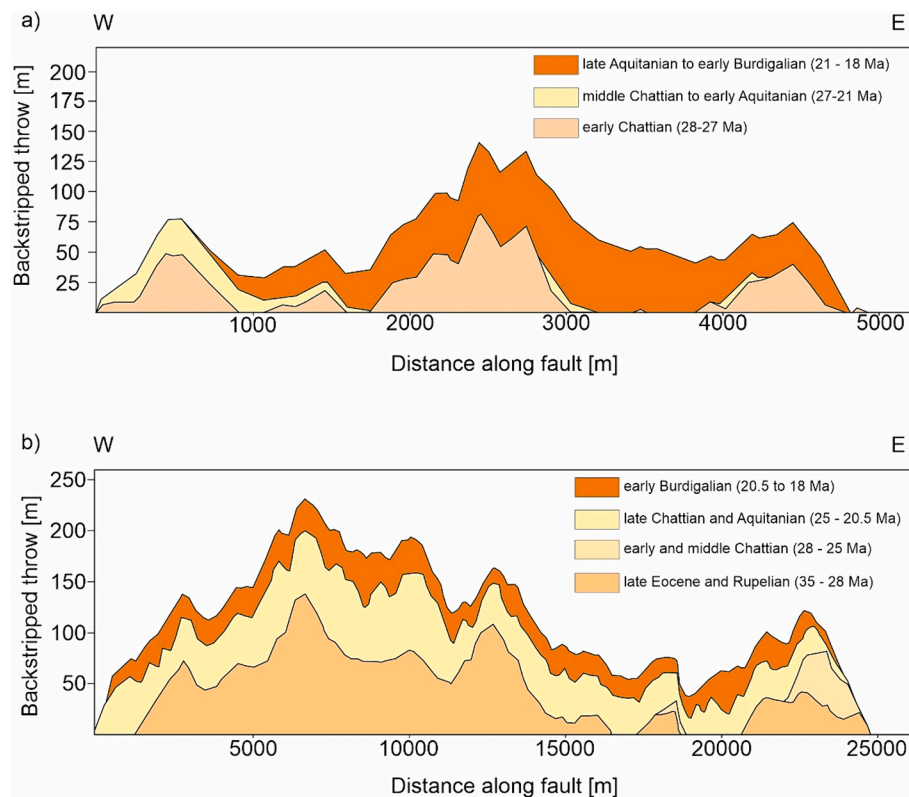


Fig. 9. Throw-length profiles of faults F1–A and F2–B. Smaller values along the vertical axis for F2–B are used because the graph would be too small otherwise. **a)** Backstripped throw-length profile for F1–A (location see Fig. 9) showing the kinematic evolution of the fault. **b)** Backstripped throw-length profile for F2–B (location see Fig. 9) showing the kinematic evolution of the fault.

normal faulting in the German Molasse. From this, and previous studies, we constrain the late Eocene basin architecture and the Oligocene to early Miocene eastward diachronous underfilled- to overfilled transition of the MB. Here, we discuss the implications of our seismic interpretations and 3D geological model for the German Molasse (Subsection 5.1). Following this, we discuss the development of the entire MB (Subsection 5.2) and possible mechanisms that drove the diachronous underfill to overfill transition in the MB (Subsection 5.3).

5.1. Tectonostratigraphic evolution of the German Molasse: along-strike variations in syn-flexural normal faulting and depositional environments

Analysis of the 3D geological model combined with seismic data volumes A and B revealed lateral heterogeneities in the basement composition underlying the German Molasse (Figs. 5, 6, and 7). The subcrop of the foreland unconformity in the Western German Molasse is characterised by Late Jurassic karstified limestones (Figs. 5 and 6). In contrast, it is characterised by Late Cretaceous deposits in the Eastern German Molasse (Figs. 5 and 7). These results agree with previous studies (Lemcke, 1988; Bachmann and Müller, 1991; von Hartmann et al., 2016; Mraz et al., 2018; Shipilin et al., 2020). Furthermore, the deep-reaching (up to 400 m) karstification of Jurassic deposits in the Western German Molasse (Fig. 6), also observed in the Swiss Molasse (Herb, 1988), implies long-lasting subaerial exposure of the basement pre-dating flexural subsidence. In contrast, karstification of the Upper Jurassic occurs only in the top 5 m in the Eastern Molasse (Köwing et al., 1968), suggesting significantly shorter subaerial exposure. Furthermore, we observed an eastward thickening of Late Cretaceous deposits in seismic volume B (Figs. 7 and A4). These lateral heterogeneities in the Mesozoic basement architecture could imply either;

1. The European margin of the future Western German Molasse experienced more intense Late Cretaceous to Eocene Alpine uplift and erosion compared to the European margin at the present-day Eastern German Molasse, or,
2. The architecture of the European margin was comprised of a paleo-high and paleo-depocenter, respectively, where the latter was buried below Cretaceous deposits after exposure to subaerial conditions.

As the Triassic to Middle Jurassic deposits are unaffected by the foreland unconformity (Fig. 5), their distribution can be used to constrain these two interpretations. Thickening of the Triassic to Middle Jurassic sediments away from a crystalline high in the Western German and eastern Swiss Molasse (Fig. 5, between 100 and 300 km) implies that this structural high existed during the earlier Mesozoic epochs. Furthermore, the Cretaceous southeast of Munich (Fig. 4c) depocenter and the paleohigh to the west can be interpreted as the Wasserburger Trog and Rhenish Shield (Fig. 10a, Lemcke, 1988). The pre-Mesozoic graben identified in our seismic dataset likely represents the Permo-Triassic Giftthal trough (Fig. 7, Bachmann and Müller, 1991). It is orientated NW-SE to the Alpine front and limited by the Landshut-Neuoetting High to the north (Bachmann and Müller, 1991). This zone of weakness partly underlies the Wasserburger Trog in the Eastern German Molasse (Fig. 10a). Therefore, we favour the 2nd hypothesis.

Pre-existing structural fabrics (e.g., horst and grabens) have been shown to lead to variations in crustal rigidity (Angrand et al., 2018). This eastward change from horst to graben-dominated domains in the pre-flexural architecture of the European margin likely caused the eastward decrease in plate strength (Andeweg and Cloetingh, 1998). Furthermore, the pre-flexural architecture of the European plate seems to have affected the Late Eocene sediment distribution in the German Molasse. This is observed as an eastward thickening of the basal neritic

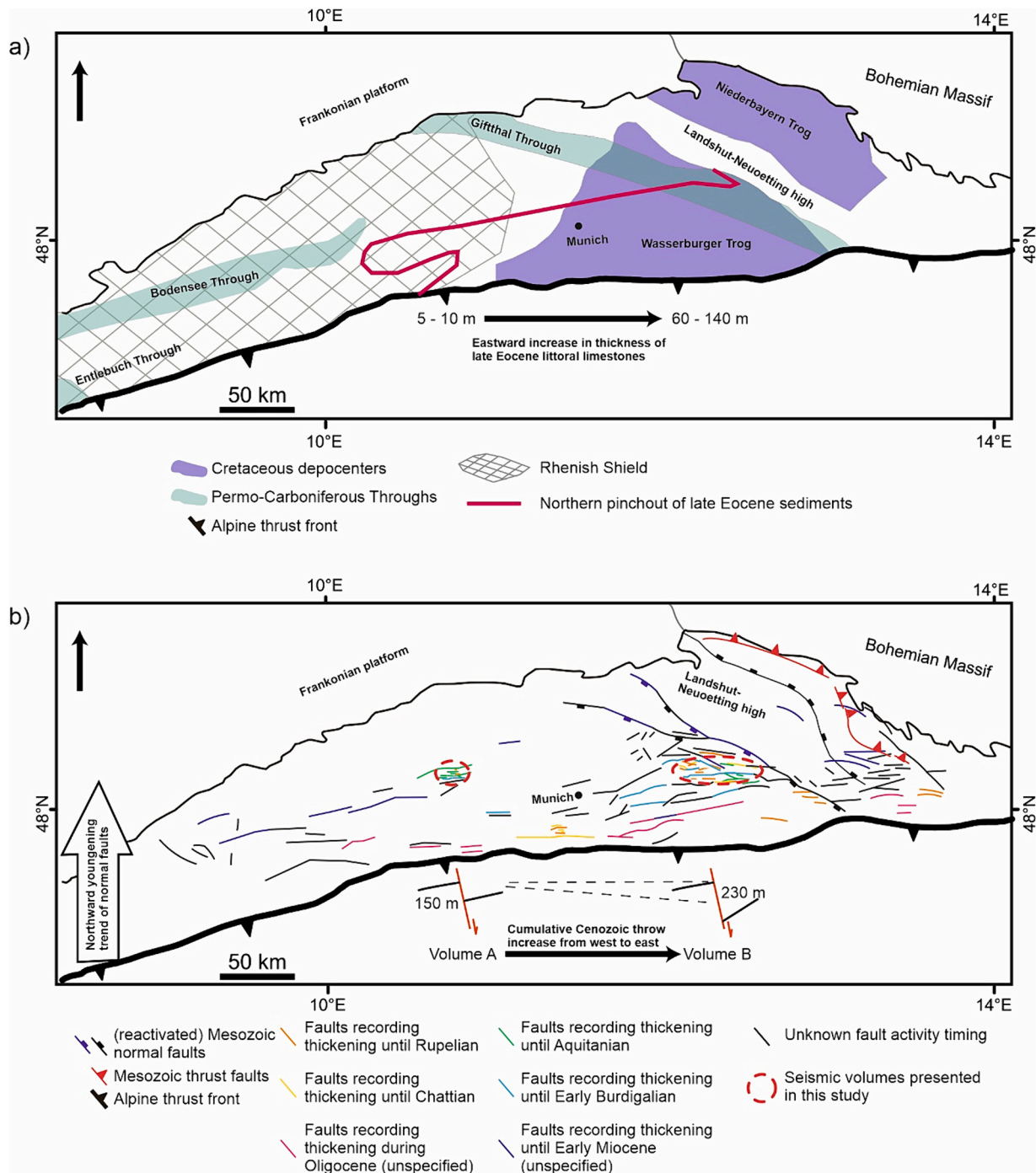


Fig. 10. a) Location of Permo-Triassic and Cretaceous depocenters underlying the foreland unconformity, the Rhenish Shield, and the northern pinchout of late Eocene sediments characterising the lowest unit of the underfilled trinity in the German Molasse. The thickness of the late Eocene littoral limestones increases from the Western German- to the Eastern German Molasse. Based on data from [Bachmann and Müller \(1991\)](#), [Lemcke \(1984\)](#), [Müller \(2011\)](#), and data presented in this study. b) Faults in the Molasse Basin, where for the syn-flexural normal faults the timing of their activity is given. Data outside the seismic volumes presented in this study is taken from ([Bachmann and Müller, 1991](#); [Mraz et al., 2018](#); [Hülscher et al., 2019](#); [Shipilin et al., 2020](#)). Faults closer to the present-day orogenic front are active until the Rupelian and Chattian, whereas faults further north are sealed by active until the Aquitanian to early Burdigalian. The cumulative Cenozoic throw value increases from west to east.

limestones corresponding to the pre-flexural horst and graben locations ([Fig. 10a](#)).

The subsequent deposition of the Rupelian Fish shales, Mergelkalk, and Bändermergel along the entire strike of the German Molasse ([Fig. 7](#), this study, [Müller, 2011](#); [Mraz et al., 2018](#); [Shipilin et al., 2020](#)) records the transition towards bathyal turbiditic conditions. This means that the influence of the inherited passive margin architecture on the

architecture of the MB had been smoothed out. The intra-Rupelian transition from bathyal to neritic deposition in the German Molasse records a decrease in relative sea level. Truncations of Rupelian reflectors against the top Rupelian ([Fig. 7](#)) suggest an association with an erosive event. This erosion coincides with both tectonic oversteepening of the distal margin observed in the Austrian Molasse ([De Ruig and Hubbard, 2006](#); [Masalimova et al., 2015](#); [Hülscher et al., 2019](#)) and a

100–150 m eustatic sea level fall at the end of the Rupelian (Haq et al., 1987). Continued progradational deposition during the early Chattian (ESE-orientated clinofolds, Figs. 7 and A6) argues against deepening due to slope oversteepening. From this, we interpret the observed incision as submarine erosion due to eustatic sea level fall at the end of the Rupelian, as suggested by Diem (1986).

During the early to middle Chattian (28 to 26 Ma), the syn-flexural normal faults in seismic volume B were mostly inactive (Fig. 9). The continued northward migration of the Alps at this time (Hinsch, 2013; Ortner et al., 2015) may have resulted in a northward migration of the forebulge and the extensional stress field around it (e.g., Supak et al., 2006; Langhi et al., 2011). This interpretation is consistent with early to middle Chattian fault activity north of seismic volume B (Fig. A14) while faults closer to the thrust front were sealed (Fig. 10b). This means the area of seismic volume B was incorporated into the axial part of the foredeep, which likely resulted in higher subsidence rates (e.g., Zweigel et al., 1998; Sinclair and Naylor, 2012). However, shallowing from neritic- to littoral conditions at this time (Chattian Sands, Fig. 7 this study, Jin et al., 1995; Zweigel et al., 1998) suggests a decrease in relative sea level. This likely occurred in response to eustatic sea level fall at the end of the Rupelian (Haq et al., 1987) combined with an increase in axially transported sediment supply derived from the Western/Central Alps (Kuhlemann, 2000) outpacing the increased flexural subsidence.

Middle Chattian juxtaposition of littoral conditions in the Eastern German Molasse (this study, Jin et al., 1995; Zweigel et al., 1998) and bathyal conditions in the Austrian Molasse (Lower Puchkirchen Fm., Wagner, 1998; De Ruig and Hubbard, 2006; Hülscher et al., 2019) led to development of the eastward facing Bavarian Shelf. Late Chattian (~ 25 Ma) NNW-directed onlap of neritic deposits onto the littoral Chattian Sands (Fig. 7) evidences a subsequent transgression of the Bavarian Shelf. Jin et al. (1995) and Zweigel et al. (1998) also observed this to the west and south of our study area. These authors attributed this flooding to a 100 m eustatic sea level rise (Haq et al., 1987). However, toplaps against the top Chattian Sands reflector (Fig. 7) spatiotemporally correlate with renewed late Chattian thrust activity observed in our study area as syn-flexural normal fault activity (Fig. 9b). Therefore, this relative sea-level rise also had a tectonic component. However, lagoonal and delta plain conditions continued to develop in the Western German Molasse (seen in seismic volume A, Figs. A10 and A13). Therefore, the westward extent of this flooding cannot exceed 100 km (distance between seismic volumes A and B). During the Aquitanian, littoral conditions migrated back to the middle Chattian position (Fig. 7). This was also observed in the study areas of Jin et al. (1995) and Zweigel et al. (1998). Taken together, this means the Bavarian Shelf remained at a relatively stable position during the late Oligocene to early Miocene (26 to 20 Ma), in accordance with Kuhlemann and Kempf (2002).

Marine conditions were re-established in the German Molasse during an early Burdigalian (~ 20–18 Ma) WNW-directed transgression (Figs. 6 and 7). This finding is consistent with results from previous authors in different parts of the MB (Strunck and Matter, 2002; Garefalakis and Schlunegger, 2019; Hülscher et al., 2019). The combination of a eustatic sea level rise (Haq et al., 1987) and a decrease in sediment supply from the hinterland (Kuhlemann, 2000) facilitated this drowning, as suggested by previous studies (Kuhlemann and Kempf, 2002; Bieg et al., 2008; Garefalakis and Schlunegger, 2019). However, early Burdigalian incision of Aquitanian sediments on the Bavarian Shelf (up to 200 m, Fig. A13), also observed in the Swiss Molasse (Schlunegger et al., 1997a; Schlunegger et al., 1997c), were likely not caused by the aforementioned decrease in sediment supply or increase in eustatic sea level. Instead, this suggests erosion due to the steepening of the distal margin of the Eastern German Molasse. Previous authors interpreted this as the result of hinterland-directed migration of the forebulge due to visco-elastic relaxation of the European plate (Zweigel et al., 1998; Hülscher

et al., 2019; Borzi et al., 2022). However, early Burdigalian syn-flexural normal fault activity in the Eastern German Molasse (Fig. 9b) suggests ongoing flexure of the European plate. This agrees with the early Burdigalian subsidence in the Western German Molasse observed by Ortner et al. (2023). Therefore, results from this study do not support the occurrence of visco-elastic relaxation of the European plate during the early Burdigalian. An alternative explanation is given in Subsection 5.3.

The syn-flexural normal faults in the German Molasse were sealed by the middle Burdigalian (Fig. 9), meaning flexure ceased at that time. Higher cumulative Cenozoic offsets in the Eastern German Molasse compared to the Western German Molasse (Fig. 9) suggest an eastward increase in the curvature of bending of the European plate.

5.2. Spatiotemporal variations in the onset of flexural subsidence and underfilled- to overfilled transition in the Molasse Basin

The obliquity between the northern pinch-out of late Eocene limestones (lower unit of underfilled trinity *sensu* Sinclair et al., 1991) and the present-day Alpine front was interpreted as resulting from along-strike variations in subsidence, controlled by the architecture of the European margin (Subsection 5.1). Considering the entire MB, the lowest unit of the underfilled trinity in the Western Molasse is only preserved in the fold and thrust belt (Helvetic nappes and the parautochthonous cover of the Aar Massif) and sparsely in the autochthonous foreland (Subsection 2.2.2 for details). This implies the autochthonous Western Molasse did not subside below sea level by the late Eocene (Fig. 11a). In contrast, in the Eastern Molasse, this unit is up to 140 m thick in the autochthonous Eastern Molasse (Fig. 7, Lemcke, 1984; Sissingh, 1997; Wagner, 1998; Zweigel et al., 1998) and is observed in the Helvetic nappes of the Eastern Alps (Heyng, 2012; Hinsch, 2013). This suggests, unlike the autochthonous Western Molasse, the autochthonous Eastern Molasse was already drowned by the late Eocene, in agreement with previous studies (Sissingh, 1997; Ziegler and Dézes, 2007). These along-strike variations in the flexural subsidence of the European plate correspond to the locations of the pre-flexural horst and graben structures (Rhenish Shield and Gifthal Trough/Wasserburger Trog, respectively, Subsection 5.1). We suggest the pre-flexural architecture of the European margin had an important influence on the late Eocene architecture of the Molasse Basin. A similar along-strike change in the early architecture of the foreland basin due to margin architecture is also observed in the Western Taiwan Foreland Basin (Chang et al., 2012), Pyrenean foreland basin (Ford et al., 2016), and Andean retro-forelands (Horton, 2018). In addition, recent work indicates that variations in passive margin architecture can also affect the underfill-to-overfill transition (Gérard et al., 2023). Certainly, post-Early Miocene along-strike variations in frontal thrusting may have added to the observed obliquity between the late Eocene deposits and the present-day Alpine thrust front, as suggested by Ortner et al. (2015).

The Rupelian stratigraphy records bathyal to neritic deposition along the entire Alpine thrust front (Figs 11b and c). However, depositional environments shallowed towards neritic and littoral conditions in the Western Molasse up to the Allgäu (31.5 to 30 Ma, Fig. 11c, Schlunegger et al., 1996; Kempf et al., 1999). This was coeval with a 200 m eustatic sea level fall (Haq et al., 1987) and the formation of alluvial megafans along the southern basin margin (Honegg-Napf, Rigi, and Speer fan systems, 31 to 30 Ma, Fig. 11c, Schlunegger et al., 1996; Kempf et al., 1999). The development of these alluvial megafans evidences topographic surface uplift in the Western/Central Alps (Kuhlemann et al., 2002), translated as increased sediment supply from this area (Kuhlemann, 2000). Together, this tectonically driven increase in sediment supply and eustatic sea level fall allowed the Western Molasse to transition from underfilled- to overfilled conditions, as suggested by previous authors (Sinclair, 1997a; Garefalakis and Schlunegger, 2018). This means the underfilled- to overfilled transition was diachronous in the

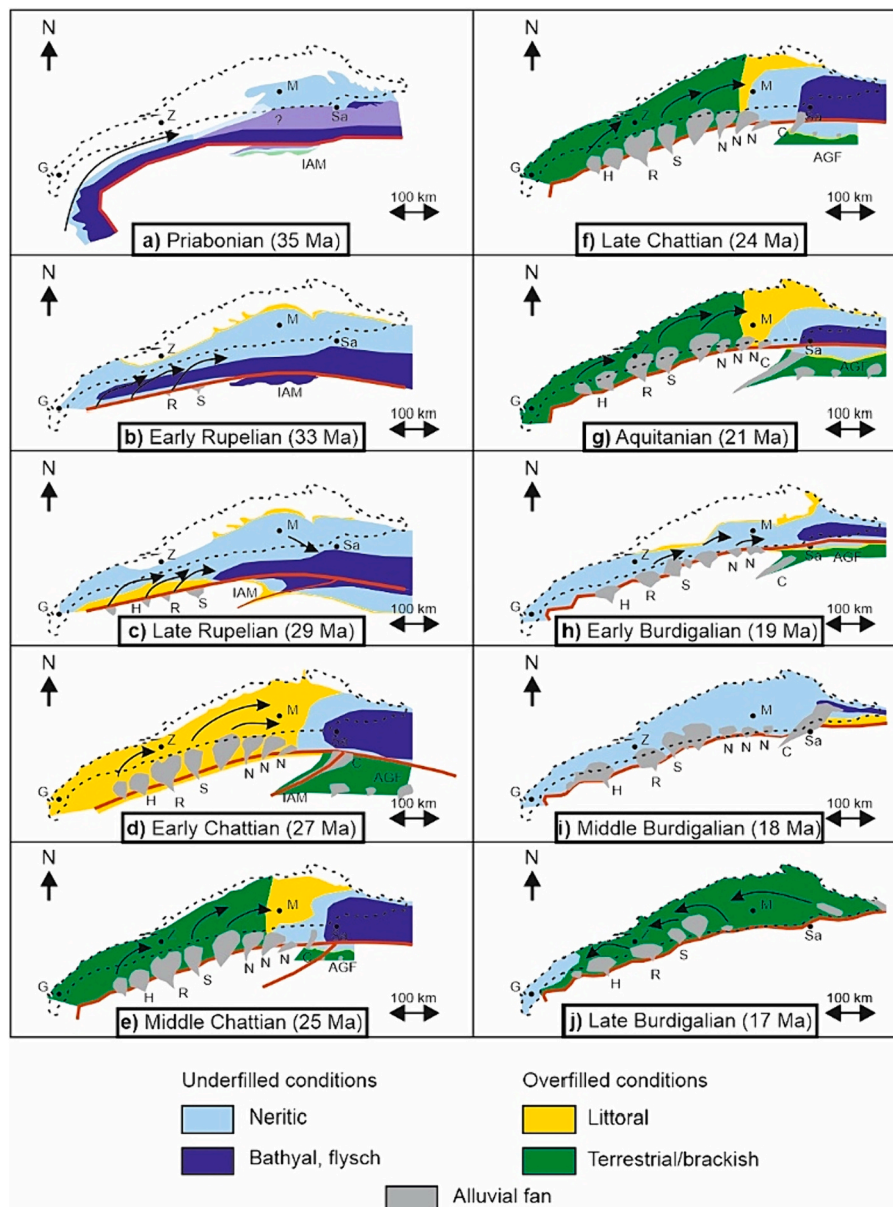


Fig. 11. Schematic paleogeographic maps of the Molasse Basin during the late Eocene, Oligocene, and early Miocene, highlighting the diachronous migration of underfill to overfill deposition and transition to homogeneous development. Black arrows indicate the direction of dominant sediment transport, a lack of arrows implies no preferred drainage direction. **a)** Priabonian (~ 35 Ma). The location and shape distributions of the Inneralpine Molasse during the Priabonian are poorly constrained and have, therefore, been made transparent. **b)** Early Rupelian (~ 33 Ma). **c)** Late Rupelian (~ 29 Ma). **d)** Early Chattian (~ 27 Ma). **e)** Middle Chattian (~ 25 Ma). **f)** Late Chattian (~ 24 Ma). **g)** Aquitanian (~ 21 Ma). **h)** Early Burdigalian (~ 19 Ma). **i)** Middle Burdigalian (~ 17 Ma). Our data was complemented with that of previous contributions (Jin et al., 1995; Sissingh, 1997; Zweigel et al., 1998; Ortner and Stingl, 2001; Kuhlemann and Kempf, 2002; Kempf and Pfiffner, 2004; Zaugg and Löpfe, 2011; Garefalakis and Schlunegger, 2019; Hülscher et al., 2019). H = Honegg-Napf fan system, R = Rigi fan system, S = Speer fan system, N = Nesselburg fans, C = Chiemgau Fan, AGF = Augenstein Formation, IAM = Inneralpine Molasse, Z = Zürich, M = Munich, S = Salzburg, G = Geneva.

Molasse Basin. Late Rupelian juxtaposition of littoral and neritic conditions in the Swiss- and Western German Molasse (Horw Sands and Rupelian Tonmergel respectively, Diem, 1986; Mraz et al., 2018) led to the development of an eastward-directed transitional zone in the Allgäu (observed as brackish deposits in Swiss Subalpine Molasse, Zaugg and Löpfe, 2011). However, axial transport of sediment derived from the Western/Central Alps allowed for the eastward migration of littoral conditions to the Bavarian Shelf by the middle Chattian (Subsection 5.1). Subsequently, the Bavarian Shelf remained relatively stable from the late Oligocene to the earliest Miocene (Subsection 5.1). This suggests that the eastward axial sediment supply was not high enough to outpace

the generation of accommodation space in the Eastern Molasse. This agrees with previous work suggesting the Bavarian Shelf was an area of sediment storage (Hülscher et al., 2021).

The MB significantly narrowed during the early Burdigalian (20 to 19 Ma, Fig. 11h). The incision of Aquitanian sediments on the Bavarian Shelf (Fig. A13) suggests that this narrowing was accompanied by erosion on the distal margin. This narrowing likely reflects hinterland-directed migration of the forebulge, as suggested by previous authors (Zweigel et al., 1998; Kuhlemann and Kempf, 2002). Furthermore, the shortening of the wavelength of flexure resulted in a deepening of the foreland basin close to the thrust front (Zweigel et al., 1998). Combined

with a rise in eustatic sea level (Haq et al., 1987) and a decrease in sediment supply from the Alpine hinterland (Kuhlemann, 2000), these processes led to a WNW-directed transgression (Fig. 6, this study, Strunck and Matter, 2002; Garefalakis and Schlunegger, 2019). Whereas neritic conditions were re-established in the Swiss and German Molasse (up to 50 m water depth, Keller, 1989; Heckeberg et al., 2010; Pippèr, 2011), bathyal conditions remained dominant in the Austrian Molasse (Fig. 11h, e.g. Lemcke, 1988; De Ruig and Hubbard, 2006; Hülscher et al., 2019).

By the late Burdigalian, the entire MB was dominated by terrestrial deposition (17 Ma, Fig. 11j). This underfill-to-overfill transition was facilitated by increased sediment supply through the uplift of the Eastern Alps and redeposition of the Augenstein Fm. (Frisch et al., 2001; Kuhlemann, 2007; Hülscher et al., 2019) coeval with the cessation of flexural subsidence (Genser et al., 2007; Ortner et al., 2015; Schlunegger and Kissling, 2022). As such, the underfill- to overfill transition in the Eastern Molasse occurred ~12 to 13.5 My later than in the Western Molasse, in rough agreement with Schlunegger and Kissling (2022). This diachronous transition was stepwise rather than continuous. The first step occurred during the late Rupelian to middle Chattian and reached as far as Munich (Figs. 11c to 11g, Kempf and Pross, 2005 and references therein). The second step occurred in the Eastern Molasse during the Burdigalian (Figs. 11h to 11j, Hülscher et al., 2019).

5.3. Mechanisms behind diachronous underfilled- to overfilled transition

Here we provide a chronology of the Alpine orogen and associated Molasse Basin evolution with attention to driving mechanisms. This is followed by an evaluation of the two hypotheses outlined in Section 1 in the context of the along-strike diachronous transition from underfilled- to overfilled conditions.

The pre-convergence European margin irregularity was characterised by the continental Briançonnais terrane in front of the future Western/Central Alps tapering out towards the future Eastern Alps (Trümpy, 1960; Faupl and Wagerich, 2000; Stampfli et al., 2002; Handy et al., 2010). Late Cretaceous to early Paleocene Alpine oceanic subduction was likely homogeneous along the entire trench (Fig. 12a and b). However, Eocene incorporation of the Briançonnais terrane into the Western/Central Alpine wedge- and slab was coeval with ongoing oceanic subduction in the Eastern Alps (Fig. 12c). Following previous results from geodynamical models of continental terrane subduction (Tetreault and Buitter, 2012; Vogt and Gerya, 2012; Li et al., 2013; Duretz et al., 2014), it is likely that the Briançonnais terrane impeded subduction along the Western/Central Alps and caused topographic uplift (Figs. 12c and 12d). Furthermore, this may have led to trench-parallel variations in convergence velocities promoting slab breakoff and tearing (Li et al., 2013; Duretz et al., 2014; Menant et al., 2016; Andrić-Tomašević et al., 2023). Therefore, the subduction- and collision of the irregular European margin likely promoted late Eocene to early Rupelian slab breakoff below the Western/Central Alps (35 Ma, von Blanckenburg and Davies, 1995; Schmid et al., 1996; Handy et al., 2015; Schlunegger and Kissling, 2022). This led to uplift of the Western/Central Alps, translated into enhanced sediment supply (Hurford, 1986; Sinclair, 1997a; Schlunegger and Willett, 1999; Von Eynatten et al., 1999; Kuhlemann, 2000; Kuhlemann, 2007; Garefalakis and Schlunegger, 2018; Schlunegger and Kissling, 2022) which forced the transition from underfilled- to overfilled conditions in the adjacent Western Molasse by the late Rupelian (Fig. 11c, Subsection 5.2). In contrast, sediment supply from the Eastern Alps remained low at the same time due to subdued topography there (Kuhlemann, 2000; Frisch et al., 2001). This promoted protracted underfilled conditions in the Eastern Molasse (Figs. 11c to 11g). The subdued topography may be explained by the Oligocene to early Miocene subduction of transitional/thinned crust (also highlighted in Le Breton et al., 2021) rather than continental

collision due to the irregularity of the European margin. It is expected that once the Eastern Alpine thrust wedge encroached onto the European plate with a “normal” thickness (~30–40 km thick), surface uplift and exhumation were enhanced. This is supported by previous analogue and numerical model results (Luth et al., 2013; Andrić et al., 2018; Vogt et al., 2018).

Late Aquitanian to early Burdigalian (20 Ma) rapid exhumation is recorded in the Eastern Alps (Fügenschuh et al., 1997; Fox et al., 2016) contemporaneous with an increase in sediment supply (Kuhlemann, 2000). Subsequently, enhanced sediment supply triggered the underfilled- to overfilled transition of the Eastern Molasse by 19 to 18 Ma (Hülscher et al., 2019; Schlunegger and Kissling, 2022). Several authors attributed these observations to a second slab breakoff (Schmid et al., 2004a; Handy et al., 2015; Schlunegger and Kissling, 2022). However, if magmatism is a fingerprint of this process (von Blanckenburg and Davies, 1995), then the absence of intrusions younger than 20 Ma would imply that the slab breakoff did not occur below the Eastern Alps at this time.

Looking at the mechanisms initiating the process of slab tearing (e.g., Rosenbaum et al., 2008; van Hunen and Allen, 2011; Andrić-Tomašević et al., 2023), the hypotheses tested in this paper (i.e., collision along the irregular margin and slab breakoff- and tearing) are linked and represent a cause-and-effect relationship. However, we question whether lateral slab breakoff- and tearing alone could cause the diachronous underfill- to overfilled transition in the Molasse Basin between ~30 and ~20 Ma. If west-to-east slab tearing occurred between 30 Ma and 20 Ma, it would be followed by a parallel younging trend in magmatism (Rosenbaum et al., 2008; Ferrari et al., 2012). However, the magmatic products in the Alps cover a time frame between 43 and 28 Ma without any orogen-parallel spatiotemporal trend (Kästle et al., 2020, their Fig. 1). The age constraints of magmatic products suggest that if slab tearing occurred, it was probably fast (a few thousand/millions of years, also suggested by Schlunegger and Kissling, 2022, their Fig. 11b). Furthermore, lateral slab tearing would lead to eastward younging of surface uplift and a gradual shallowing of the foreland basin along the strike as proposed by Meulenkamp et al. (1996) and Van der Meulen et al. (1998). Instead, the stepwise diachronous underfill-to-overfill transition in the Molasse Basin (Subsection 5.2) argues against continuous and slow lateral slab tearing between ~30 and 20 Ma.

The Eastern Alpine wedge overthrusting of the Bohemian Spur (acting as a buttress) was coeval with the onset of out-of-sequence thrusting (Covault et al., 2009; Hinsch, 2013; Ortner et al., 2015), surface uplift in the hinterland (Beidinger and Decker, 2014; Heberer et al., 2023a; Heberer et al., 2023b), and cessation of subsidence in the Eastern Molasse after 20 Ma (Genser et al., 2007; Schlunegger and Kissling, 2022). A stepping back of deformation led to uplift- and erosion of the Augenstein Fm. (Frisch et al., 2001; Hülscher et al., 2021). With frontal thrusting “locked”, continued indentation of the Adriatic plate led to internal Eastern Alpine thickening (observed as the rapid early Miocene exhumation of the Tauern Window, Fügenschuh et al., 1997; Scharf et al., 2013; Favaro et al., 2015; Fox et al., 2016). This tectonically-driven uplift led to increased sediment supply from the Eastern Alps (Kuhlemann, 2000), which subsequently forced the underfilled- to overfilled transition in the Eastern Molasse by 19–18 Ma (Hülscher et al., 2019). Furthermore, the southward shift of the topographic loading due to internal thickening led to hinterland-directed migration of the forebulge, causing early Burdigalian incision of the northern basin margin (Fig. A13). Uplift of the Molasse Basin above the Bohemian Spur (Heberer et al., 2023a; Heberer et al., 2023b) coeval with ongoing subsidence of the German- and Swiss Molasse (which we observe as ongoing normal fault activity, Schlunegger and Kissling, 2022; Ortner et al., 2023) caused a reversal in the drainage direction (Kuhlemann and Kempf, 2002; Garefalakis and Schlunegger, 2019). This highlights slab breakoff- and tearing are not necessary to explain the evolution of the

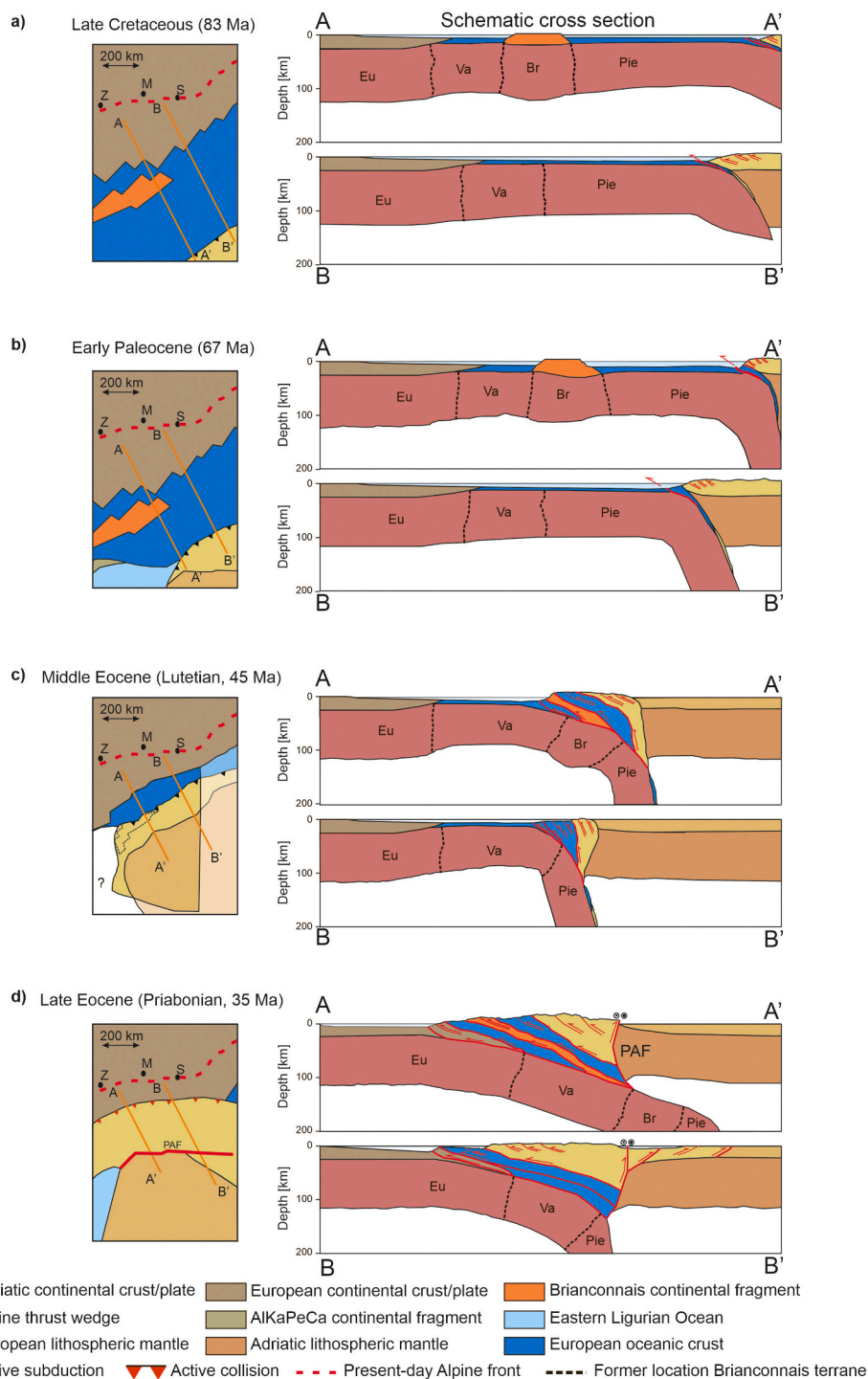


Fig. 12. Paleogeographic reconstructions and respective cross sections of the convergent tectonics between the late Cretaceous and late Eocene, based on paleogeographic reconstructions from previous authors (Stampfli et al., 2002; Handy et al., 2010; Handy et al., 2015). **a)** In the late Cretaceous, the subduction of the Piemont Ocean under Austroalpine nappes starts. These nappes were located on the northern margin of the Adriatic plate. **b)** In the early Paleocene, subduction of the Piemont Ocean under the Adriatic plate continues along-strike the entire trench. This resulted in a homogeneous European slab. **c)** By the Middle Eocene, the continental Briançonnais terrane was subducted below and incorporated into the future Western/Central Alpine thrust wedge. To the east, oceanic subduction was uninterrupted. **d)** During the late Eocene, continental collision between the Adriatic and European plates occurred. Like the Middle Eocene, along-strike variations in the architecture of the European slab still existed. The segmentation of the Western/Central Alpine slab into oceanic and continental fragments may have promoted late Eocene to early Oligocene slab breakoff- and tearing.

Eastern Alps- and Molasse during the early Miocene. However, we admit that with available data, this model cannot explain the Southern Alps changing from retro-wedge to pro-wedge deformation after 20 Ma through a subduction polarity reversal associated with European slab breakoff at ~20 Ma (Handy et al., 2015; Eizenhöfer et al., 2023). Further investigations into this topic are needed.

The above discussion highlights how subduction- and collision of the irregular European margin could have induced the diachronous flysch to molasse transition in the Molasse Basin. However, these models have not incorporated the effects of both the global Eocene-Oligocene and Oligocene-Miocene cooling events (Miller et al., 1991; Liu et al., 2009) on the erosion- and sediment supply. The transitions from underfilled- to overfilled conditions in both the Western and Eastern Molasse temporally correspond to these global cooling events. Moreover, such global cooling events have been shown to enhance erosion in mountainous areas (e.g., Herman et al., 2013). Therefore, we suggest that for future research climatic effects on denudation rates should be considered.

6. Conclusions

This study analysed along-strike variations in the Mesozoic basement, sedimentary fill, and syn-flexural normal fault kinematics of the MB. Our analysis provides insight into the lithospheric- and crustal-scale processes responsible for the diachronous underfilled- to overfilled transition during the Oligocene to early Miocene. The main conclusions include:

- The German Molasse was partitioned into a structural high and a depocenter in the west and east, respectively. Both these features existed since the Mesozoic and influenced the late Eocene basin architecture. By the Rupelian, this effect was smoothed out as recorded by homogeneous depositional environments along-strike the entire Molasse Basin.
- Increased sediment supply from the Western/Central Alps at the end of the Rupelian (31.5 to 30 Ma) allowed the underfilled- to overfilled transition to occur in the Western Molasse. However, low sediment supply from the Eastern Alps and eastward axial transport of sediments derived from the Western/Central Alps, respectively, was insufficient to force the underfilled- to overfilled transition in the Eastern Molasse.
- The Bavarian Shelf remained at a relatively stationary position between the Middle Chattian (26 Ma) and the end of the Aquitanian (20.5 Ma).
- A west-to-east increase in cumulative Cenozoic offsets along syn-flexural normal faults suggests a higher Cenozoic curvature of bending of the European plate in the Eastern German Molasse compared to the Western German Molasse.

- Subduction- and collision of the irregular European margin promoted late Eocene to early Oligocene slab breakoff, leading to an increase in surface uplift of the Western/Central Alps but not the Eastern Alps. Consequentially, the enhanced sediment supply from this uplift led to an overfilling of the Western Molasse, whereas underfilled conditions remained dominant in the Eastern Molasse. By the early Miocene, deformation may have been forced back into the core of the Eastern Alps because of the architecture of the European margin. This led to an enhanced sediment supply from the Eastern Alps, causing an overfilling of the Eastern Molasse.

CRedit authorship contribution statement

Lucas H.J. Eskens: Writing – original draft, Visualization, Methodology, Investigation, Formal analysis, Conceptualization. **Nevena Andrić-Tomašević:** Writing – original draft, Supervision, Funding acquisition, Conceptualization. **Peter M. Süß:** Writing – original draft, Supervision, Methodology. **Matthias Müller:** Writing – review & editing, Resources. **Rolf Herrmann:** Writing – review & editing, Resources. **Todd A. Ehlers:** Writing – review & editing, Supervision.

Declaration of competing interest

The authors declare that they have no known competing financial interests or personal relationships that could have appeared to influence the work reported in this paper.

Data availability

The data that has been used is confidential.

Acknowledgements

This study was supported by the Deutsche Forschungsgemeinschaft (DFG) grant to Nevena Andrić-Tomašević (TO 1364/1-1) and Todd A. Ehlers (EH 329/24-1) under the priority program 4D-MB and is a contribution to the AlpArray initiative. A * in the text denotes that the software is a product of SLB to which we were given access for academic purposes. We also want to thank the geological surveys from Bavaria, Baden-Württemberg, Austria, and Switzerland for providing the GEO-MOL data. Furthermore, we thank the Bavarian Geological Survey for providing additional 2D seismic data. Furthermore, we would like to thank Fritz Schlunegger and an anonymous reviewer for constructive comments during the review process. Lastly, the manuscript benefitted from discussions with Eline Le Breton (FU Berlin), Mark Handy (FU Berlin), Arthur Borzi (FU Berlin), and Hugo Ortner (University of Innsbruck).

Appendix A

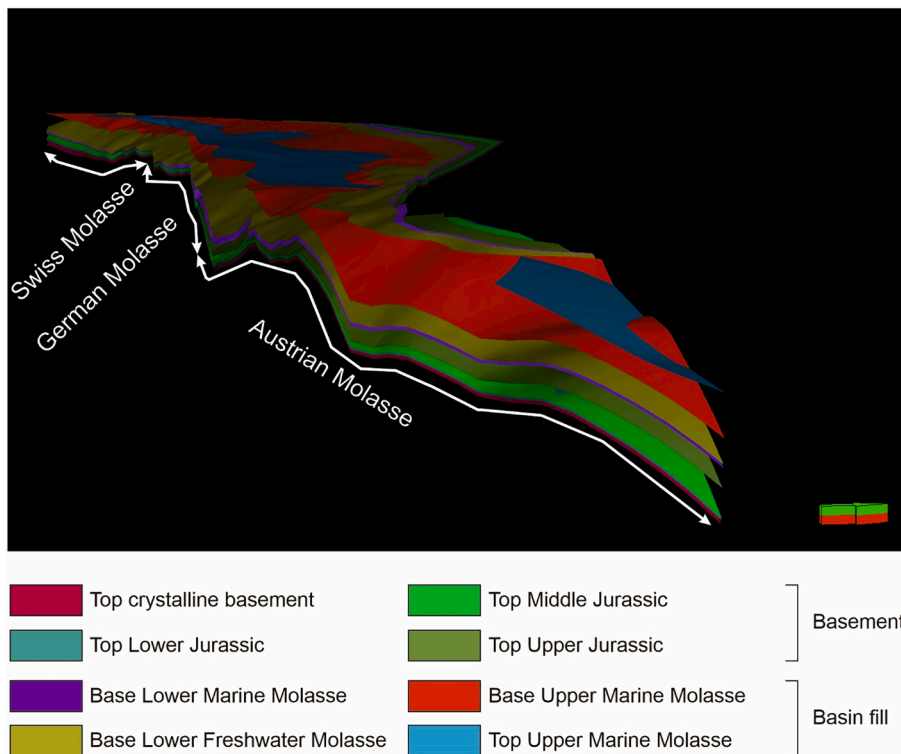


Fig. A1. 3D view of the low-resolution geological model of the entire Molasse Basin.

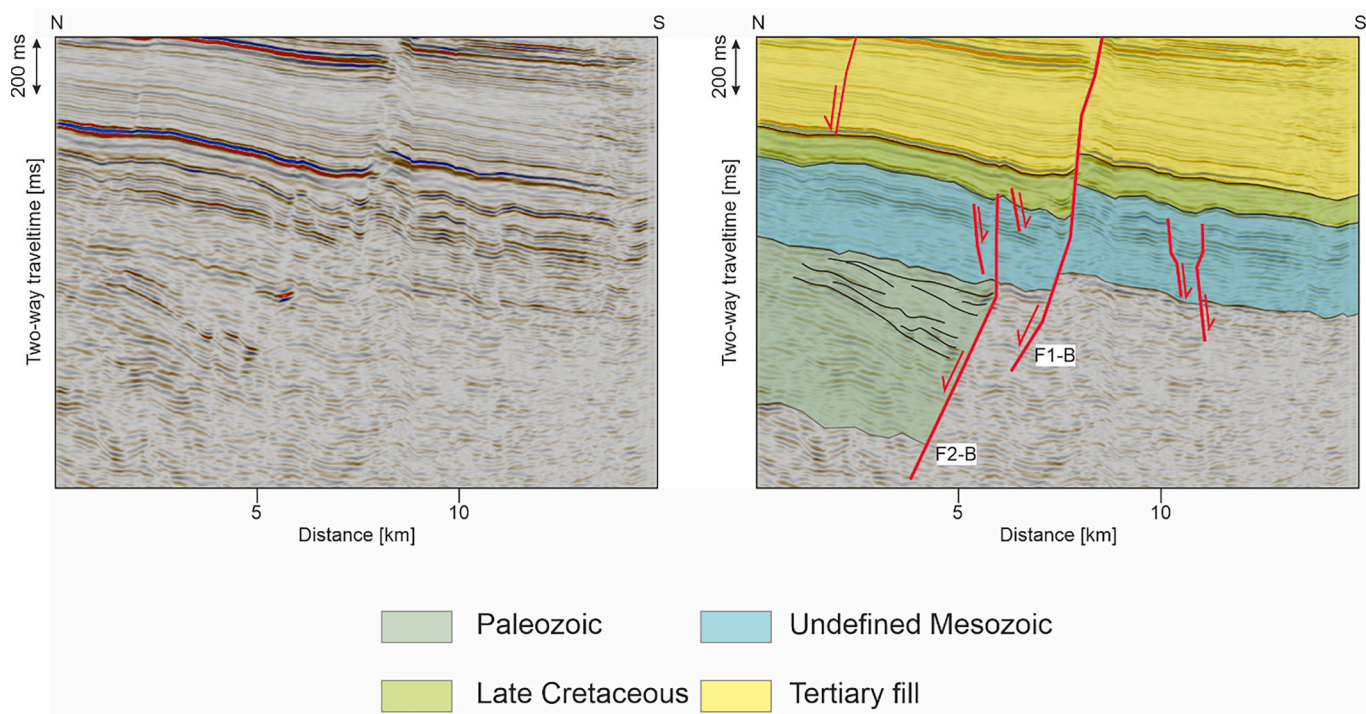


Fig. A2. Uninterpreted and interpreted N-S seismic lines through seismic volume B. Interpreted line highlights the presence of a fault-bounded Permo-Triassic graben in the study area. This line is given in the time domain, as the depth conversion below the late Cretaceous is inaccurate.

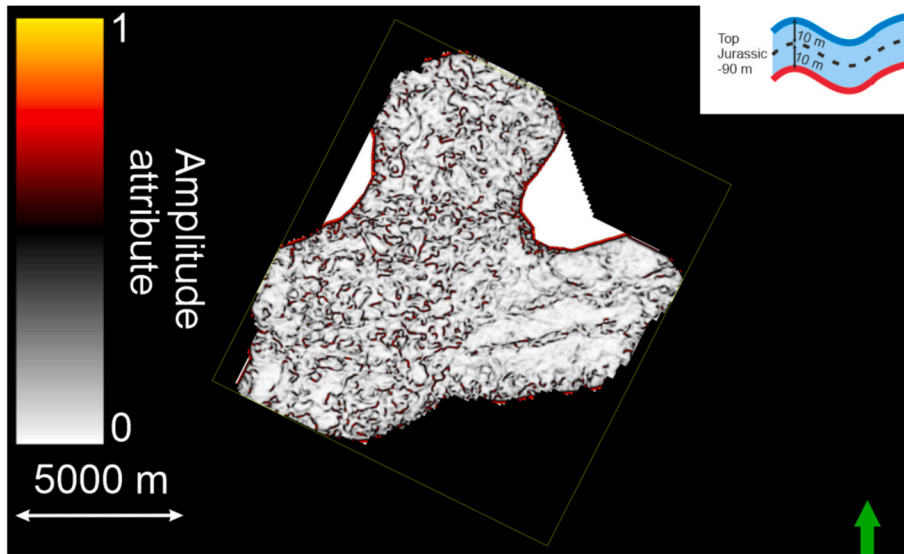


Fig. A3. Variance attribute map of the Upper Jurassic seismic-stratigraphic body in seismic volume A with a thickness of 20 m. The WNW shows a chaotic distribution of high variance values, which is characteristic of heavily karstified limestones. To the ESE, a patch of dominantly low variance values indicates that the Upper Malm is not (as heavily) karstified here.

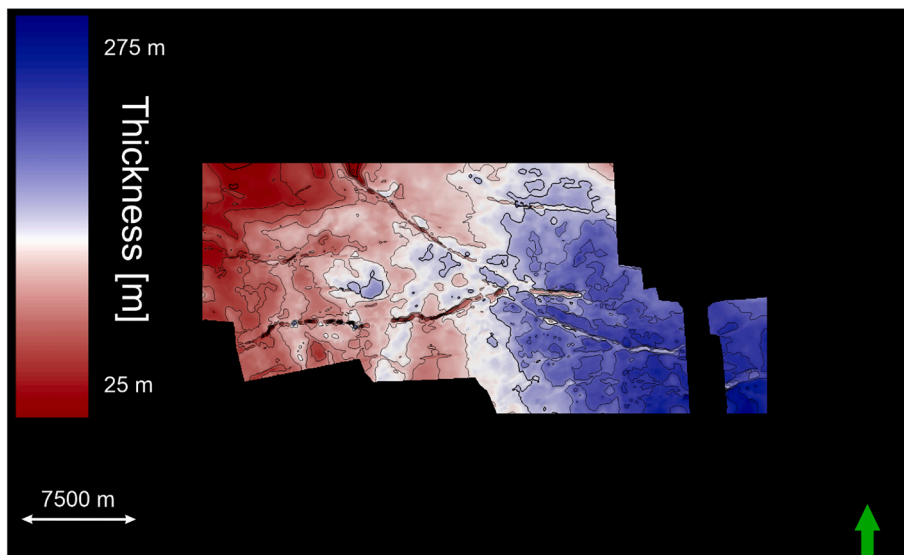


Fig. A4. Thickness distribution of the post-Turonian late Cretaceous seismic-stratigraphic body in seismic volume B.

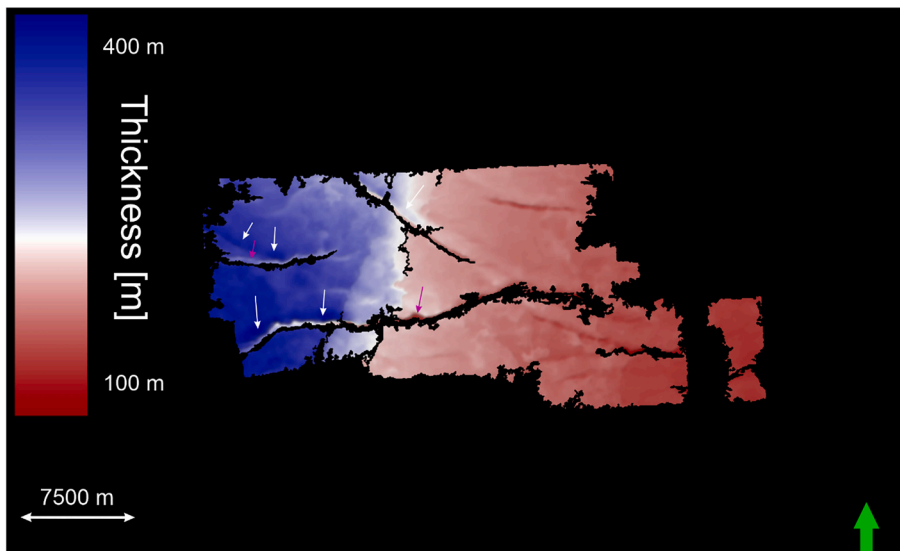


Fig. A5. Thickness distribution of the Rupelian seismic-stratigraphic body in seismic volume B. White arrows indicate the thickening of the Rupelian towards the faults, and purple arrows indicate locations of thickness artefacts when creating isopachs.

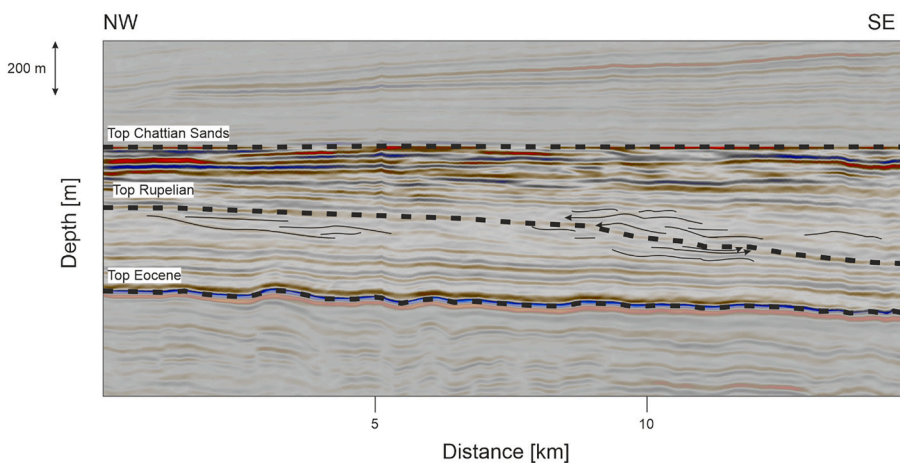


Fig. A6. SE dipping Clinoforms (black solid lines) in the Upper Rupelian and Lower Chattian seismic stratigraphy in volume B. Arrows indicate reflector terminations.

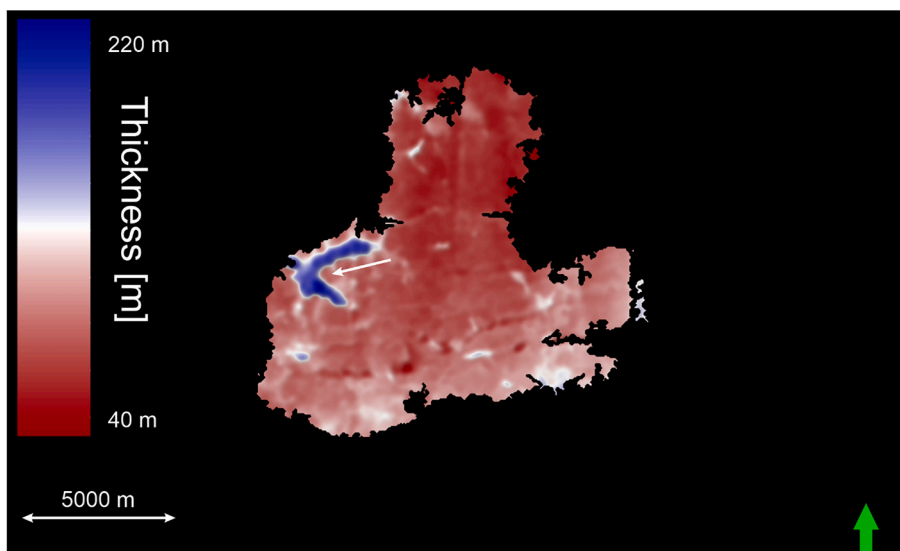


Fig. A7. Thickness distribution of the Early Chattian seismic-stratigraphic body in seismic volume A. White arrow highlights the local increase in thickness related to karstification of underlying Upper Jurassic limestones.

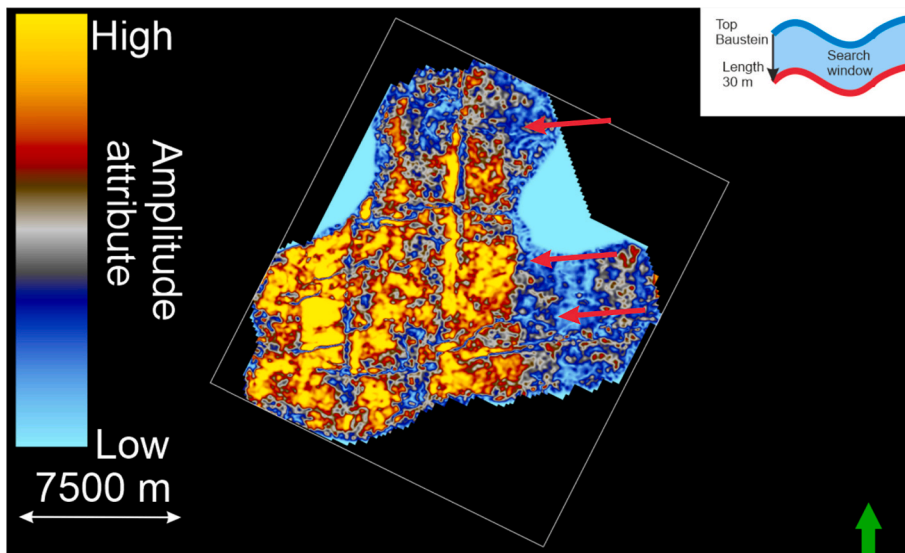


Fig. A8. Sweetness map of the Early Chattian seismic stratigraphic unit in volume A. High amplitudes indicate more sandy areas, and low amplitudes indicate more muddy areas. As such, the N-S bands of high and low sweetness values are interpreted to highlight the orientation of a N-S directed coastline. The western side was a more shallow and sandy area. In contrast, the eastern side is more mud-rich and was likely located in a deeper water depositional environment. Red arrows indicate the direction of onlap.

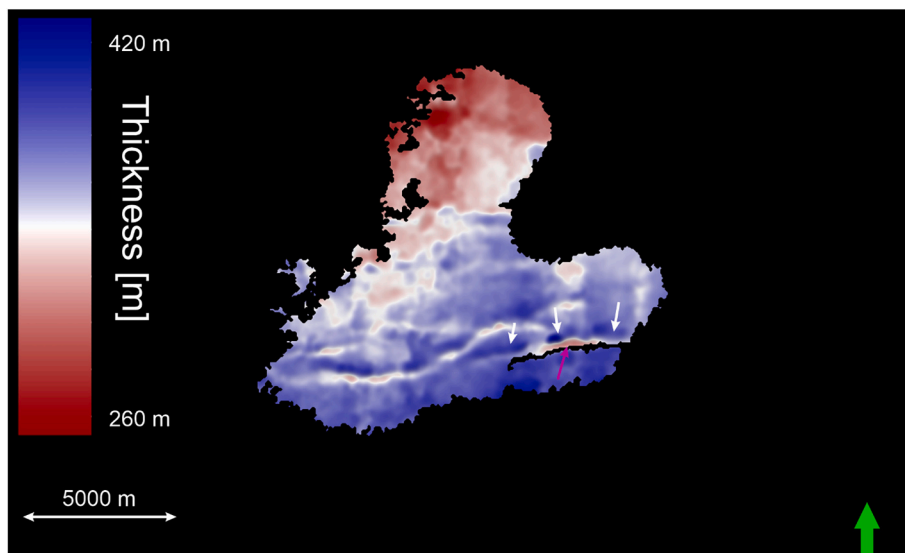


Fig. A9. Thickness distribution of the Cyrena Beds in seismic volume A. White arrows indicate thickening towards the faults, and purple arrows indicate locations of thickness artefacts when creating isopachs.

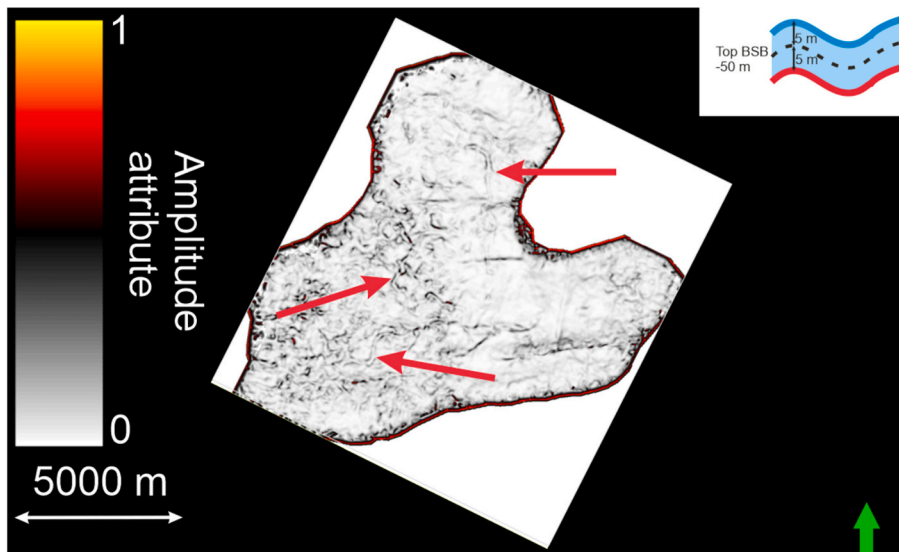


Fig. A10. Variance attribute map of the Cyrena Beds in seismic volume A with a thickness of 10 m. Red arrows highlight curving bands of high variance values indicate meandering channels.

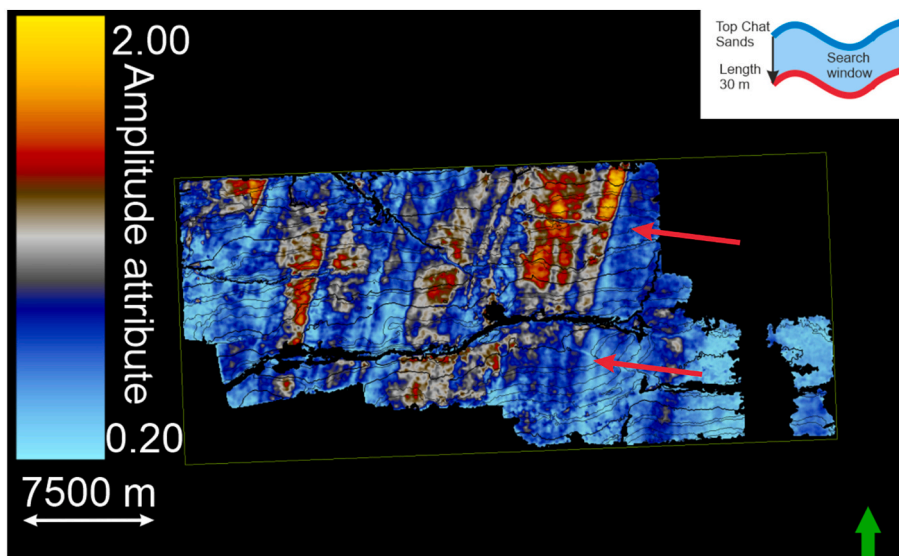


Fig. A11. Sweetness map of the Middle Chattian seismic stratigraphic unit in volume B. High amplitudes indicate more sandy areas, low amplitudes indicate more muddy areas. As such, the NE-SW bands of high and low sweetness values are interpreted to highlight the orientation of an NE-SW directed coastline. The western side was a more shallow and sandy area. In contrast, the eastern side is more mud-rich and was likely located in a deeper water depositional environment. Red arrows indicate the direction of onlap.

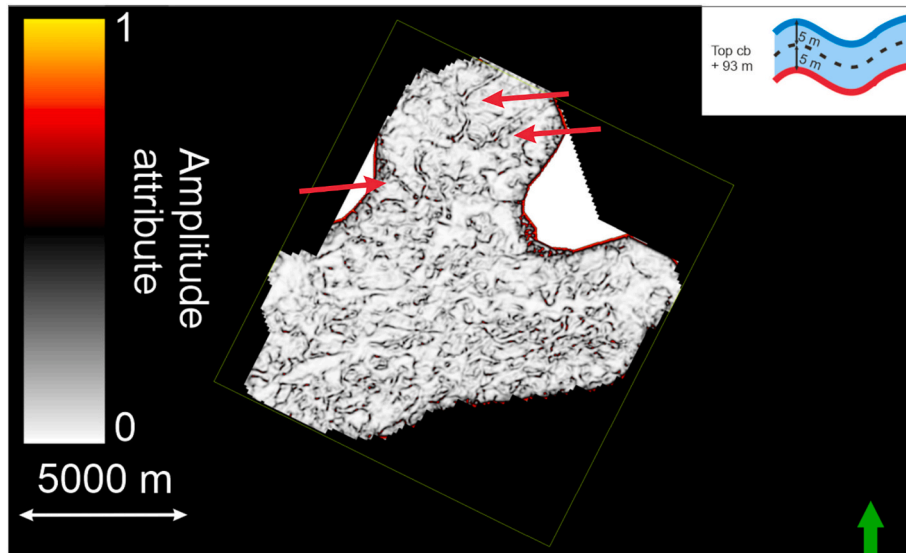


Fig. A12. Variance attribute map of the late Aquitanian reflectors in seismic volume A with a thickness of 10 m. Red arrows highlight curving bands of high variance values highlighting the positions of meandering channels.

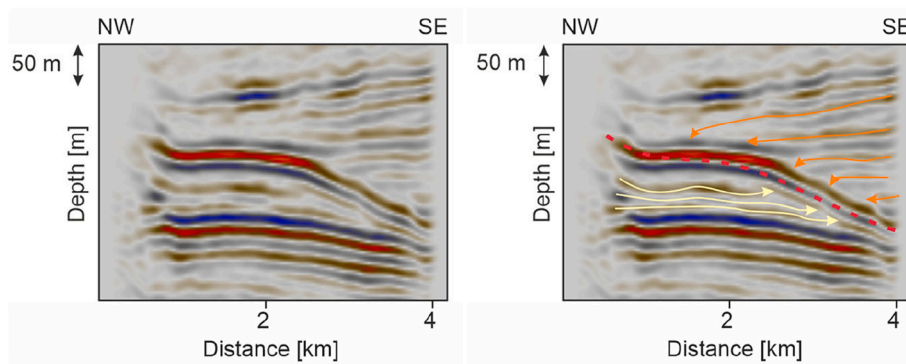


Fig. A13. Uninterpreted and interpreted parts of an NW-SE trending seismic line in seismic volume B at the western edge of the Austrian Molasse. Yellow arrows mark terminating Aquitanian reflectors, the red dashed line the BHU, and orange arrows onlapping Early Burdigalian reflectors. For location see Fig. 7.

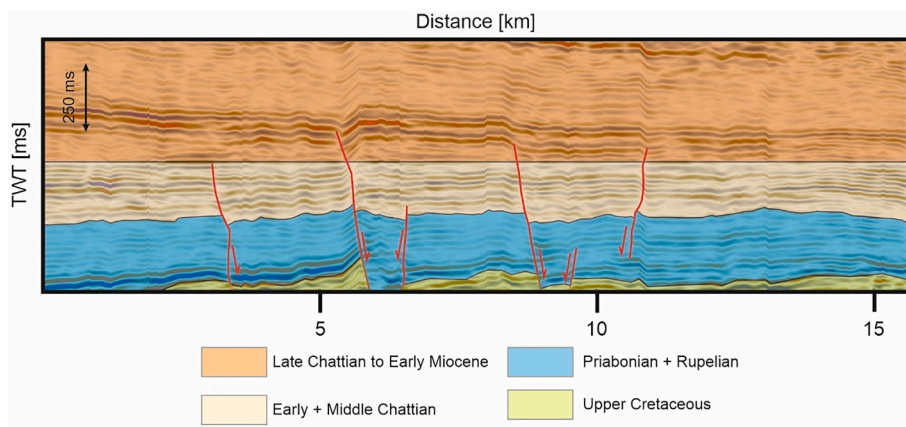


Fig. A14. Interpreted section flattened on the top Chattian Sands reflector. Red lines indicate syn-flexural normal faults. Thickness changes of the early to Middle Chattian stratigraphy indicate these normal faults were active during the deposition of this unit. For location see Fig. 1a.

A.1. Time to depth conversion of seismic volume B

The seismic data in volume B is in the time domain, which does not give true geometries and, thus, not true fault throws. To produce a time-depth conversion, reflectors were picked in the time domain using welltops where checkshots are available. Based on borehole data, the depth of the stratigraphic surfaces is locally known. Where interpreted time surfaces intersect with wells that drill the corresponding surface, it is possible to calculate average seismic velocities from the surface to the reflector of interest (Table A1). Based on the average velocities of the separate horizons, an overall average velocity of 2678 m/s was calculated from the surface until the top Turonian reflector.

Table A1
Average velocities from the surface to interpreted seismic horizon.

Stratigraphic surface	Average velocity (m/s)	Number of wells
Base Hall Unconformity	2709	93
Top Chattian Sands	2516	91
Base Eocene	2729	63
Top Turonian	2739	10

This velocity was used to convert the seismic data from the time to the depth domain. Reflectors and faults were then picked on the depth-converted seismics. These interpretations were used to calculate T-x profiles for seismic volume B.

References

- Alipour, M., 2023. Collision along irregular plate margin controlled the tectono-stratigraphic evolution of the Iranian Zagros fold and thrust belt. *Mar. Pet. Geol.* 154, 106311.
- Allen, P.A., Crampton, S.L., Sinclair, H.D., 1991. The inception and early evolution of the North Alpine Foreland Basin, Switzerland. *Basin Res.* 3 (3), 143–163.
- Amante, C., Eakins, B.W., 2009. ETOPO1 arc-minute global relief model: procedures, data sources and analysis.
- Amadori, C., Toscani, G., Di Giulio, A., Maesano, F.E., D'Ambrogio, C., Ghielmi, M., Fantoni, R., 2019. From cylindrical to non-cylindrical foreland basin: Pliocene–Pleistocene evolution of the Po Plain–Northern Adriatic basin (Italy). *Basin Res.* 31 (5), 991–1015.
- Andeweg, B., Cloetingh, S., 1998. Flexure and 'unflexure' of the North Alpine German–Austrian.
- Andrić, N., Vogt, K., Matenco, L., Cvetković, V., Cloetingh, S., Gerya, T., 2018. Variability of orogenic magmatism during Mediterranean-style continental collisions: a numerical modelling approach. *Gondwana Res.* 56, 119–134.
- Andrić-Tomašević, N., Koptev, A., Maiti, G., Gerya, T., Ehlers, T.A., 2023. Slab tearing in non-collisional settings: Insights from thermo-mechanical modelling of oblique subduction. *Earth Planet. Sci. Lett.* 610, 118907.
- Angrand, P., Ford, M., Watts, A.B., 2018. Lateral variations in foreland flexure of a rifted continental margin: the Aquitaine Basin (SW France). *Tectonics* 37 (2), 430–449.
- Ascione, A., Ciarcia, S., Di Donato, V., Mazzoli, S., Vitale, S., 2012. The Pliocene–Quaternary wedge-top basins of southern Italy: an expression of propagating lateral slab tear beneath the Apennines. *Basin Res.* 24 (4), 456–474.
- Bachmann, G.H., Müller, M., 1991. The Molasse basin, Germany: evolution of a classic petroliferous foreland basin. Generation, accumulation, and production of Europe's hydrocarbons. Special publication of the European association of petroleum geoscientists. *Eur. Assoc. Pet. Geosci. Spec. Publ.* 1, 263–276.
- Barth, S., Oberli, F., Meier, M., 1989. U—Th—Pb systematics of morphologically characterized zircon and allanite: a high-resolution isotopic study of the Alpine Renssen pluton (northern Italy). *Earth Planet. Sci. Lett.* 95 (3–4), 235–254.
- Beaumont, C., 1981. Foreland basins. *Geophys. J. Int.* 65 (2), 291–329.
- Beidinger, A., Decker, K., 2014. Quantifying early Miocene in-sequence and out-of-sequence thrusting at the Alpine-Carpathian junction. *Tectonics* 33 (3), 222–252.
- Bieg, U., Süß, M.P., Kuhlemann, J., 2008. Simulation of tidal flow and circulation patterns in the early Miocene (Upper Marine Molasse) of the Alpine foreland basin. In: *Analogue and Numerical Modelling of Sedimentary Systems: From Understanding to Prediction*, 40, pp. 145–169.
- von Blanckenburg, F., Davies, J., 1992. Slab breakout. Explanation of mantle magmatism in the Alps? *Trans. Am. Geophys. Union Eos* 73, 546.
- von Blanckenburg, F., Davies, J.H., 1995. Slab breakout: a model for syn-collisional magmatism and tectonics in the Alps. *Tectonics* 14 (1), 120–131.
- Borzi, A., McPhee, P., Hülscher, J., LeBreton, E., Handy, M.R., Bernhard, A., 2022. Major Neogene shift in the structural and sedimentary evolution of the North Alpine Foreland Basin. In: *6th Annual AlpArray Scientific Meeting*, Prague.
- Bry, M., White, N., Singh, S., England, R., Trowell, C., 2004. Anatomy and formation of oblique continental collision: South Falkland basin. *Tectonics* 23 (4).
- Burkhard, M., 1988. L'Helvétique de la bordure occidentale du massif de l'Aar (évolution tectonique et métamorphique). *Eclogae Geol. Helv.* 81 (1), 63–114.
- Burkhard, M., Sommaruga, A., 1998. Evolution of the western Swiss Molasse basin: structural relations with the Alps and the Jura belt. *Geol. Soc. Lond. Spec. Publ.* 134 (1), 279–298.
- Caputo, R., Poli, M.E., Zanferrari, A., 2010. Neogene–Quaternary tectonic stratigraphy of the eastern Southern Alps, NE Italy. *J. Struct. Geol.* 32 (7), 1009–1027.
- Cartwright, J.A., Mansfield, C., Trudgill, B., 1996. The growth of normal faults by segment linkage. *Geol. Soc. Lond. Spec. Publ.* 99 (1), 163–177.
- Caumon, G., Mallet, J.-L., 2006. 3D Stratigraphic models: representation and stochastic modelling. In: *Int. Assoc. for Mathematical Geology—XIIth International Congress*, 4p.
- Chang, J.-H., Yu, H.-S., Hsu, H.-H., Liu, C.-S., 2012. Forebulge migration in late Cenozoic Western Taiwan foreland basin. *Tectonophysics* 578, 117–125.
- Chapman, T., Meneilly, A., 1991. The displacement patterns associated with a reverse-reactivated, normal growth fault. *Geol. Soc. Lond. Spec. Publ.* 56 (1), 183–191.
- Cooper, M., Addison, F., Alvarez, R., Coral, M., Graham, R., Hayward, A., Howe, S., Martinez, J., Naar, J., Peñas, R., 1995. Basin development and tectonic history of the Llanos Basin, Eastern Cordillera, and middle Magdalena Valley, Colombia. *AAPG Bull.* 79 (10), 1421–1442.
- Covault, J.A., Hubbard, S.M., Graham, S.A., Hinsch, R., Linzer, H.-G., 2009. Turbidite-reservoir architecture in complex foredeep-margin and wedge-top depocenters, Tertiary Molasse foreland basin system, Austria. *Mar. Pet. Geol.* 26 (3), 379–396.
- Dal-Piaz, G.V., Del-Moro, A., Martin, S., Venturelli, G., 1988. Post-collisional magmatism in the Ortler-Cevedale massif (Northern Italy). *Jahrb. Geol. Bundesanst.* 131 (4), 533–551.
- De Ruig, M.J., Hubbard, S.M., 2006. Seismic facies and reservoir characteristics of a deep-marine channel belt in the Molasse foreland basin, Puchkirchen Formation, Austria. *AAPG Bull.* 90 (5), 735–752.
- DeCelles, P.G., 2012. Foreland basin systems revisited: Variations in response to tectonic settings. In: *Tectonics of Sedimentary Basins: Recent Advances*, pp. 405–426.
- DeCelles, P.G., Giles, K.A., 1996. Foreland basin systems. *Basin Res.* 8 (2), 105–123.
- DeCelles, P.G., Mitra, G., 1995. History of the Sevier orogenic wedge in terms of critical taper models, Northeast Utah and Southwest Wyoming. *Geol. Soc. Am. Bull.* 107 (4), 454–462.
- Dewey, J., Kidd, W., 1974. Continental collisions in the Appalachian-Caledonian orogenic belt: Variations related to complete and incomplete suturing. *Geology* 2 (11), 543–546.
- Diem, B., 1986. Die Untere Meeresmolasse zwischen der Saane (Westschweiz) und der Ammer (Oberbayern). *Eclogae Geol. Helv.* 79 (2), 493–559.
- von Doppler, G., Heissig, K., Reichenbacher, B., 2005. Die Gliederung des Tertiärs im süddeutschen Molassebecken.
- Duret, T., Gerya, T., Spakman, W., 2014. Slab detachment in laterally varying subduction zones: 3-D numerical modeling. *Geophys. Res. Lett.* 41 (6), 1951–1956.
- Eizenhöfer, P.R., Glotzbach, C., Kley, J., Ehlers, T.A., 2023. Thermo-kinematic evolution of the eastern European Alps along the TRANSALP transect. *Tectonics* e2022TC007380.
- Faupl, P., Wagreich, M., 2000. Late Jurassic to Eocene palaeogeography and geodynamic evolution of the Eastern Alps. *Mitteilungen Österreichischer Geol. Gesellschaft* 92 (1999), 79–94.
- Favaro, S., Schuster, R., Handy, M.R., Scharf, A., Pestal, G., 2015. Transition from orogen-perpendicular to orogen-parallel exhumation and cooling during crustal indentation—Key constraints from 147Sm/144Nd and 87Rb/87Sr geochronology (Tauern Window, Alps). *Tectonophysics* 665, 1–16.
- Ferrari, L., 2004. Slab detachment control on mafic volcanic pulse and mantle heterogeneity in Central Mexico. *Geology* 32 (1), 77–80.
- Ferrari, L., Orozco-Esquivel, T., Manea, V., Manea, M., 2012. The dynamic history of the Trans-Mexican Volcanic Belt and the Mexico subduction zone. *Tectonophysics* 522, 122–149.
- Flemings, P.B., Jordan, T.E., 1989. A synthetic stratigraphic model of foreland basin development. *J. Geophys. Res. Solid Earth* 94 (B4), 3851–3866.
- Flemings, P.B., Jordan, T.E., 1990. Stratigraphic modeling of foreland basins: interpreting thrust deformation and lithosphere rheology. *Geology* 18 (5), 430–434.
- Ford, M., Hemmer, L., Vacherat, A., Gallagher, K., Christophoul, F., 2016. Retro-wedge foreland basin evolution along the ECORS line, eastern Pyrenees, France. *J. Geol. Soc.* 173 (3), 419–437.
- Fox, M., Herman, F., Willett, S.D., Schmid, S.M., 2016. The exhumation history of the European Alps inferred from linear inversion of thermochronometric data. *Am. J. Sci.* 316 (6), 505–541.
- Frisch, W., 1979. Tectonic progradation and plate tectonic evolution of the Alps. *Tectonophysics* 60 (3–4), 121–139.
- Frisch, W., Kuhlemann, J., Dunkl, I., Székely, B., 2001. The Dachstein paleosurface and the Augenstein Formation in the Northern Calcareous Alps—a mosaic stone in the geomorphological evolution of the Eastern Alps. *Int. J. Earth Sci.* 90, 500–518.
- Fügenshuh, B., Seward, D., Mancktelow, N., 1997. Exhumation in a convergent orogen: the western Tauern window. *Terra Nova* 9 (5–6), 213–217.
- Garefalakis, P., Schlunegger, F., 2018. Link between concentrations of sediment flux and deep crustal processes beneath the European Alps. *Sci. Rep.* 8 (1), 183.
- Garefalakis, P., Schlunegger, F., 2019. Tectonic processes, variations in sediment flux, and eustatic sea level recorded by the 20 Myr old Burdigalian transgression in the Swiss Molasse basin. *Solid Earth* 10 (6), 2045–2072.
- Gautschi, A., Schnellmann, M., Albert, W., Blümling, P., Viator, T., Blaser, P., Müller, H., 2008. Nagra Technischer Bericht 08–04: Vorschlag geologischer Standortgebiete für das SMA- und das HAA-Lager.
- Genser, J., Cloetingh, S.A., Neubauer, F., 2007. Late orogenic rebound and oblique Alpine convergence: new constraints from subsidence analysis of the Austrian Molasse basin. *Glob. Planet. Chang.* 58 (1–4), 214–223.
- GeoMol, 2015. GeoMol – Assessing subsurface potentials of the Alpine Foreland Basins for sustainable planning and use of natural resources. *Proj. Rep.* 188.

- Gérard, B., Rouby, D., Huisman, R.S., Robin, C., Fillon, C., Braun, J., 2023. Impact of Inherited Foreland Relief on Retro-Foreland Basin Architecture. *J. Geophys. Res. Solid Earth* 128 (3) e2022JB024967.
- Govers, R., Wortel, M.J.R., 2005. Lithosphere tearing at STEP faults: response to edges of subduction zones. *Earth Planet. Sci. Lett.* 236 (1–2), 505–523.
- Großmann, J., Hofmann, N., Pamer, R., Spörlein, T., Pechnig, R., Knapp, D., Clauser, K., Karp, T., Günther, D., 2024. Abgeschlossene Arbeiten zur Digitalisierung geophysikalischer Grundlagendaten in Bayern. *Geologica Bavarica* 127, 1–77.
- Gül, M., Gürbüz, K., Cronin, B.T., 2015. Irregular plate boundary controls on foreland basin sedimentation (Miocene, Kahramanmaraş Foreland Basin, SE Turkey). *J. Asian Earth Sci.* 111, 804–818.
- Handy, M.R., Schmid, S.M., Bousquet, R., Kissling, E., Bernoulli, D., 2010. Reconciling plate-tectonic reconstructions of Alpine Tethys with the geological–geophysical record of spreading and subduction in the Alps. *Earth Sci. Rev.* 102 (3–4), 121–158.
- Handy, M.R., Ustaszewski, K., Kissling, E., 2015. Reconstructing the Alps–Carpathians–Dinarides as a key to understanding switches in subduction polarity, slab gaps and surface motion. *Int. J. Earth Sci.* 104 (1), 1–26.
- Haq, B.U., Hardenbol, J., Vail, P.R., 1987. Chronology of fluctuating sea levels since the Triassic. *Science* 235 (4793), 1156–1167.
- von Hartmann, H., Tanner, D.C., Schumacher, S., 2016. Initiation and development of normal faults within the German alpine foreland basin: the inconspicuous role of basement structures. *Tectonics* 35 (6), 1560–1574.
- He, B., Jiao, C., Xu, Z., Cai, Z., Zhang, J., Liu, S., Li, H., Chen, W., Yu, Z., 2016. The paleotectonic and paleogeography reconstructions of the Tarim Basin and its adjacent areas (NW China) during the late early and Middle Paleozoic. *Gondwana Res.* 30, 191–206.
- Heberer, B., Bernhard, S., István, D., Reinhard, S., Tari, G., Wagreich, M., von Hagke, C., Wessely, G., 2023a. Rapid Oligocene to Miocene Cooling in the Easternmost Alps Driven by Thrusting onto the Bohemian Promontory and/or Deep Mantle Processes, Copernicus Meetings.
- Heberer, B., Salcher, S., Tari, G., Wessely, G., Dunkl, I., Sachsenhofer, R., Wagreich, M., von Hsgke, C., 2023b. The Impact of the Bohemian Spur on the Cooling and Exhumation Pattern of the Eastern Alpine Wedge, 4DMB, Bad Hofgastein.
- Heckeberg, N., Pipperr, M., Lüchli, B., Heimann, F.U., Reichenbacher, B., 2010. The Upper Marine Molasse (Burdigalian, Otnangian) in Southwest Germany-facies interpretation and a new lithostratigraphic terminology. *Zeitschrift Deutschen Gesellschaft Geowissenschaften* 161 (3), 285.
- Heimann, F.U., Schmid, D.U., Pipperr, M., Reichenbacher, B., 2009. Re-interpreting the Baltringer Horizont as a subtidal channel facies: Implications for a new understanding of the Upper Marine Molasse “Cycles” (early Miocene). *Neues Jahrbuch Geol. Paläontol.-Abhandlungen* 254 (1), 135.
- Herb, R., 1988. Eocaena Paläogeographie und Paläotektonik des Helvetikums. *Eclogae Geol. Helv.* 81 (3), 611–657.
- Herman, F., Seward, D., Valla, P.G., Carter, A., Kohn, B., Willett, S.D., Ehlers, T.A., 2013. Worldwide acceleration of mountain erosion under a cooling climate. *Nature* 504 (7480), 423–426.
- Herrmann, P., Draxler, I., Müller, M., 1985. Erläuterungen zu Blatt 83 Sulzberg. *Geologische (Bundesanstalt)* 83, 1–20.
- Heuberger, S., Roth, P., Zingg, O., Naef, H., Meier, B.P., 2016. The St. Gallen Fault Zone: a long-lived, multiphase structure in the North Alpine Foreland Basin revealed by 3D seismic data. *Swiss J. Geosci.* 109 (1), 83–102.
- Heyng, A., 2012. Lithostratigraphie der Adelholzen-Formation (Eozän, Lutetium) im Raum Siegsdorf (Oberbayern). Verlag Documenta Naturae.
- Hinsch, R., 2013. Laterally varying structure and kinematics of the Molasse fold and thrust belt of the Central Eastern Alps: Implications for exploration. *AAPG Bull.* 97 (10), 1805–1831.
- Homewood, P., Lateltin, O., 1988. Classic swiss clastics (flysch and molasse) the alpine connection. *Geodin. Acta* 2 (1), 1–11.
- Homewood, P., Allen, P., Williams, G., 1986. Dynamics of the Molasse Basin of Western Switzerland. Foreland basins. Blackwell Scientific Publications, Oxford, UK, pp. 199–217.
- Horton, B.K., 2018. Sedimentary record of Andean mountain building. *Earth Sci. Rev.* 178, 279–309.
- Hülscher, J., Fischer, G., Grunert, P., Auer, G., Bernhardt, A., 2019. Selective Recording of Tectonic Forcings in an Oligocene/Miocene Submarine Channel System: Insights from New Age Constraints and Sediment Volumes from the Austrian Northern Alpine Foreland Basin. *Front. Earth Sci.* 7 (302).
- Hülscher, J., Sobel, E.R., Verwater, V., Groß, P., Chew, D., Bernhardt, A., 2021. Detrital apatite geochemistry and thermochronology from the Oligocene/Miocene Alpine foreland record the early exhumation of the Tauern Window. *Basin Res.* 33 (6), 3021–3044.
- van Hunen, J., Allen, M.B., 2011. Continental collision and slab breakoff: a comparison of 3-D numerical models with observations. *Earth Planet. Sci. Lett.* 302 (1–2), 27–37.
- Hurford, A.J., 1986. Cooling and uplift patterns in the Lepontine Alps South Central Switzerland and an age of vertical movement on the Insubric fault line. *Contrib. Mineral. Petrol.* 92 (4), 413–427.
- Hurford, A., Flisch, M., Jäger, E., 1989. Unravelling the thermo-tectonic evolution of the Alps: a contribution from fission track analysis and mica dating. *Geol. Soc. Lond. Spec. Publ.* 45 (1), 369–398.
- Jackson, C.A.-L., Bell, R.E., Rotevatn, A., Tvedt, A.B., 2017. Techniques to determine the kinematics of synsedimentary normal faults and implications for fault growth models. *Geol. Soc. Lond. Spec. Publ.* 439 (1), 187–217.
- Jin, J., Aigner, T., Luterbacher, H., Bachmann, G.H., Müller, M., 1995. Sequence stratigraphy and depositional history in the south-eastern German Molasse Basin. *Mar. Pet. Geol.* 12 (8), 929–940.
- Kästle, E.D., Rosenberg, C., Boschi, L., Bellahsen, N., Meier, T., El-Sharkawy, A., 2020. Slab breakoffs in the Alpine subduction zone. *Int. J. Earth Sci.* 109 (2), 587–603.
- Keller, B., 1989. Fazies und stratigraphie der Oberen Meeresmolasse (unteres Miozän) zwischen Napf und Bodensee.
- Kempf, O., Pfiffner, O.A., 2004. Early Tertiary evolution of the North Alpine Foreland Basin of the Swiss Alps and adjoining areas. *Basin Res.* 16 (4), 549–567.
- Kempf, O., Pross, J., 2005. The lower marine to lower freshwater Molasse transition in the northern Alpine foreland basin (Oligocene; Central Switzerland–south Germany): age and geodynamic implications. *Int. J. Earth Sci.* 94 (1), 160–171.
- Kempf, O., Matter, A., Burbank, D., Mange, M., 1999. Depositional and structural evolution of a foreland basin margin in a magnetostratigraphic framework: the eastern Swiss Molasse Basin. *Int. J. Earth Sci.* 88 (2), 253–275.
- Koson, S., Chenrai, P., Chooiwong, M., 2013. Seismic attributes and their applications in seismic geomorphology. *Bull. Earth Sci. Thailand* 6 (1), 1–9.
- Köwing, K., Kraus, L., Rückert, G., 1968. Erläuterungen zur Geologischen Karte von Bayern, 1, p. 25000.
- Kuhlemann, J., 2000. Post-collisional sediment budget of circum-Alpine basins (Central Europe). *Mem. Sci. Geol. Padova* 52 (1), 1–91.
- Kuhlemann, J., 2007. Paleogeographic and paleotopographic evolution of the Swiss and Eastern Alps since the Oligocene. *Glob. Planet. Chang.* 58 (1–4), 224–236.
- Kuhlemann, J., Kempf, O., 2002. Post-Eocene evolution of the North Alpine Foreland Basin and its response to Alpine tectonics. *Sediment. Geol.* 152 (1–2), 45–78.
- Kuhlemann, J., Frisch, W., Székely, B., Dunkl, I., Kazmer, M., 2002. Post-collisional sediment budget history of the Alps: tectonic versus climatic control. *Int. J. Earth Sci.* 91, 818–837.
- Langhi, L., Ciftci, N.B., Borel, G.D., 2011. Impact of lithospheric flexure on the evolution of shallow faults in the Timor foreland system. *Mar. Geol.* 284 (1–4), 40–54.
- Lash, G.G., 1988. Along-strike variations in foreland basin evolution: possible evidence for continental collision along an irregular margin. *Basin Res.* 1 (2), 71–83.
- Le Breton, E., Brune, S., Ustaszewski, K., Zahirovic, S., Seton, M., Müller, R.D., 2021. Kinematics and extent of the Piemont–Liguria Basin—implications for subduction processes in the Alps. *Solid Earth* 12 (4), 885–913.
- Lemcke, K., 1984. Geologische Vorgänge in den Alpen ab Obereozän im Spiegel vor allem der deutschen Molasse. *Geol. Rundsch.* 73 (1), 371–397.
- Lemcke, K., 1988. Das bayerische Alpenvorland vor der Eiszeit.
- Li, Z.-H., Xu, Z., Gerya, T., Burg, J.-P., 2013. Collision of continental corner from 3-D numerical modeling. *Earth Planet. Sci. Lett.* 380, 98–111.
- Lihou, J.C., Allen, P.A., 1996. Importance of inherited rift margin structures in the early North Alpine Foreland Basin, Switzerland. *Basin Res.* 8 (4), 425–442.
- Liu, Z., Pagani, M., Zinniker, D., DeConto, R., Huber, M., Brinkhuis, H., Shah, S.R., Leckie, R.M., Pearson, A., 2009. Global cooling during the Eocene-Oligocene climate transition. *Science* 323 (5918), 1187–1190.
- Luth, S., Willingshofer, E., Sokoutis, D., Cloetingh, S., 2013. Does subduction polarity changes below the Alps? Inferences from analogue modelling. *Tectonophysics* 582, 140–161.
- Malkowski, M.A., Sharman, G.R., Graham, S.A., Fildani, A., 2017. Characterisation and diachronous initiation of coarse clastic deposition in the Magallanes–Austral foreland basin, Patagonian Andes. *Basin Res.* 29, 298–326.
- Mallet, J.-L., 2004. Space–time mathematical framework for sedimentary geology. *Math. Geol.* 36 (1), 1–32.
- Manatschal, G., Chenin, P., Hauptert, I., Masini, E., Frasca, G., Decarlis, A., 2022. The importance of rift inheritance in understanding the early collisional evolution of the Western Alps. *Geosciences* 12 (12), 434.
- Mansfield, C., Cartwright, J., 1996. High resolution fault displacement mapping from three-dimensional seismic data: evidence for dip linkage during fault growth. *J. Struct. Geol.* 18 (2–3), 249–263.
- Masalimova, L.U., Lowe, D.R., Mchargue, T., Derksen, R., 2015. Interplay between an axial channel belt, slope gullies and overbank deposition in the Puchkirchen Formation in the Molasse Basin, Austria. *Sedimentology* 62 (6), 1717–1748.
- Matter, A., 1980. Flysch und Molasse of Western and Central Switzerland. Wepf & Co. Maurer, H., 2006. Rekonstruktion der Ablagerungsverhältnisse im nordalpinen Vorlandbecken Südwest-Deutschlands.
- Menant, A., Sternai, P., Jolivet, L., Guillou-Frottier, L., Gerya, T., 2016. 3D numerical modeling of mantle flow, crustal dynamics and magma genesis associated with slab roll-back and tearing: the eastern Mediterranean case. *Earth Planet. Sci. Lett.* 442, 93–107.
- Menkveld-Gfeller, U., 1995. Stratigraphie, Fazies und Pelogeographie des Eozäns der helvetischen Decken der Westschweiz (Diablerets- und Wildhorn-Decke). *Eclogae Geol. Helv.* 88, 115–134.
- Menkveld-Gfeller, U., 1997. Die Bürgen-Fm. und die Klimeshorn-Fm.: Formelle Definition zweier lithostratigraphischer Einheiten des Eozäns der helvetischen Decken. *Eclogae Geol. Helv.* 90, 245–261.
- Meulenkamp, J., Kováč, M., Cicha, I., 1996. On late Oligocene to Pliocene depocentre migrations and the evolution of the Carpathian-Pannonian system. *Tectonophysics* 266 (1–4), 301–317.
- Meyer, R.K., Schmidt-Kaler, H., 1990. Paläogeographie und Schwammriffentwicklung des süddeutschen Malm—ein Überblick. *Facies* 23 (1), 175–184.
- Miller, K.G., Wright, J.D., Fairbanks, R.G., 1991. Unlocking the ice house: Oligocene-Miocene oxygen isotopes, eustasy, and margin erosion. *J. Geophys. Res. Solid Earth* 96 (B4), 6829–6848.
- Mohn, G., Manatschal, G., Müntener, O., Beltrando, M., Masini, E., 2010. Unravelling the interaction between tectonic and sedimentary processes during lithospheric thinning in the Alpine Tethys margins. *Int. J. Earth Sci.* 99 (1), 75–101.
- Mohn, G., Manatschal, G., Beltrando, M., Hauptert, I., 2014. The role of rift-inherited hyper-extension in Alpine-type orogens. *Terra Nova* 26 (5), 347–353.

- Mraz, E., Moeck, I., Bissmann, S., Hild, S., 2018. Multiphase fossil normal faults as geothermal exploration targets in the Western Bavarian Molasse Basin: Case study Mauerstetten. *Z. Dtsch. Ges. Geowiss.* 169 (3), 389–411.
- Müller, M., 2011. Die Geologie beiderseits des Lechs im Raum Schongau. *Geologica Bavarica*.
- Nachtmann, W., Wagner, L., 1987. Mesozoic and early Tertiary evolution of the Alpine foreland in Upper Austria and Salzburg, Austria. *Tectonophysics* 137 (1–4), 61–76.
- Neely, J.S., Furlong, K.P., 2018. Evidence of displacement-driven maturation along the San Cristobal Trough transform plate boundary. *Earth Planet. Sci. Lett.* 485, 88–98.
- Ortner, H., Stingl, V., 2001. Facies and Basin Development of the Oligocene in the Lower Inn Valley (Tyrol/Bavaria).
- Ortner, H., Aichholzer, S., Zerlauth, M., Pilser, R., Fügenschuh, B., 2015. Geometry, amount, and sequence of thrusting in the Subalpine Molasse of western Austria and southern Germany, European Alps. *Tectonics* 34 (1), 1–30.
- Ortner, H., von Hagke, C., Sommaruga, A., Mock, S., Mosar, J., Hirsch, R., Beidinger, A., 2023. The Northern Deformation Front of the European Alps, The Alpine Chain. *ISTE-Wiley*, London.
- Petersen, K., Clausen, O., Korstgård, J., 1992. Evolution of a salt-related listric growth fault near the D-1 well, block 5605, Danish North Sea: displacement history and salt kinematics. *J. Struct. Geol.* 14 (5), 565–577.
- Pfiffner, A., 1986. Evolution of the North Alpine Foreland Basin in the Central Alps, 8. The International Association of Sedimentologists, pp. 219–228.
- Pfiffner, O.A., 1993. The structure of the Helvetic nappes and its relation to the mechanical stratigraphy. *J. Struct. Geol.* 15 (3–5), 511–521.
- Pippèr, M., 2011. Characterisation of Otnangian (middle Burdigalian) palaeoenvironments in the North Alpine Foreland Basin using benthic foraminifera—a review of the Upper Marine Molasse of southern Germany. *Mar. Micropaleontol.* 79 (3–4), 80–99.
- Platt, N.H., 1992. Fresh-water carbonates from the lower Freshwater Molasse (Oligocene, western Switzerland): sedimentology and stable isotopes. *Sediment. Geol.* 78 (1–2), 81–99.
- Platt, N.H., Keller, B., 1992. Distal alluvial deposits in a foreland basin setting—the lower Freshwater Miocene, Switzerland: sedimentology, architecture and palaeosols. *Sedimentology* 39 (4), 545–565.
- Ratschbacher, L., Merle, O., Davy, P., Cobbold, P., 1991. Lateral extrusion in the Eastern Alps, part 1: boundary conditions and experiments scaled for gravity. *Tectonics* 10 (2), 245–256.
- Reichenbacher, B., Uhlir, U., Kowalke, T., Bassler, B., Matzke-Karasz, R., Schenk, B., 2004. Biota, palaeoenvironments and biostratigraphy of continental Oligocene deposits of the south German Molasse Basin (Penzberg syncline). *Palaeogeology* 47 (3), 639–677.
- Robson, A., King, R., Holford, S., 2017. Structural evolution of a gravitationally detached normal fault array: Analysis of 3D seismic data from the Ceduna Sub-Basin, Great Australian Bight. *Basin Res.* 29 (5), 605–624.
- Rögl, F., Hochuli, P., Müller, C., 1979. Oligocene–early Miocene stratigraphic correlations in the Molasse Basin of Austria. *Annales Geologiques des Pays Helleniques. Tome Hors Ser.* 30, 1045–1050.
- Rosenbaum, G., Gasparon, M., Lucente, F.P., Peccerillo, A., Miller, M.S., 2008. Kinematics of slab tear faults during subduction segmentation and implications for Italian magmatism. *Tectonics* 27 (2) n/a/n/a.
- Rosenberg, C., Brun, J.P., Cagnard, F., Gapais, D., 2007. Oblique indentation in the Eastern Alps: Insights from laboratory experiments. *Tectonics* 26 (2).
- Rosenberg, C.L., Bellahsen, N., Rabaute, A., Girault, J.B., 2021. Distribution, style, amount of collisional shortening, and their link to Barrovian metamorphism in the European Alps. *Earth Sci. Rev.* 222.
- Roure, F., 2008. Foreland and hinterland basins: what controls their evolution? *Swiss J. Geosci.* 101 (1), 5–29.
- Rowan, M.G., Hart, B.S., Nelson, S., Flemings, P.B., Trudgill, B.D., 1998. Three-dimensional geometry and evolution of a salt-related growth-fault array: Eugene Island 330 field, offshore Louisiana, Gulf of Mexico. *Marin. Petrol. Geol.* 15 (4), 309–328.
- Scharf, A., Handy, M., Favaro, S., Schmid, S.M., Bertrand, A., 2013. Modes of orogen-parallel stretching and extensional exhumation in response to microplate indentation and roll-back subduction (Tauern Window, Eastern Alps). *Int. J. Earth Sci.* 102 (6), 1627–1654.
- Schlunegger, F., Castellort, S., 2016. Immediate and delayed signal of slab breakoff in Oligo/Miocene Molasse deposits from the European Alps. *Sci. Rep.* 6 (1), 1–11.
- Schlunegger, F., Kissling, E., 2015. Slab rollback orogeny in the Alps and evolution of the Swiss Molasse basin. *Nat. Commun.* 6 (1), 1–10.
- Schlunegger, F., Kissling, E., 2022. Slab load controls beneath the Alps on the source-to-sink sedimentary pathways in the Molasse basin. *Geosciences* 12 (6), 226.
- Schlunegger, F., Willett, S., 1999. Spatial and temporal variations in exhumation of the central Swiss Alps and implications for exhumation mechanisms. *Geol. Soc. Lond. Spec. Publ.* 154 (1), 157–179.
- Schlunegger, F., Burbank, D., Matter, A., Engesser, B., Mödden, C., 1996. Magnetostratigraphic calibration of the Oligocene to Middle Miocene (30–15 Ma) mammal biozones and depositional sequences of the Swiss Molasse Basin. *Eclogae Geol. Helv.* 89 (2), 753–788.
- Schlunegger, F., Leu, W., Matter, A., 1997a. Sedimentary sequences, seismic facies, subsidence analysis, and evolution of the Burdigalian Upper Marine Molasse Group, Central Switzerland. *AAPG Bull.* 81 (7), 1185–1207.
- Schlunegger, F., Matter, A., Burbank, D., Klaper, E., 1997b. Magnetostratigraphic constraints on relationships between evolution of the central Swiss Molasse basin and Alpine orogenic events. *Geol. Soc. Am. Bull.* 109 (2), 225–241.
- Schlunegger, F., Matter, A., Burbank, D., Leu, W., Mange, M., Matyas, J., 1997c. Sedimentary sequences, seismofacies and evolution of depositional systems of the Oligo/Miocene lower Freshwater Molasse Group, Switzerland. *Basin Res.* 9 (1), 1–26.
- Schmid, S.M., Pfiffner, O.-A., Froitzheim, N., Schönborn, G., Kissling, E., 1996. Geophysical-geological transect and tectonic evolution of the Swiss-Italian Alps. *Tectonics* 15 (5), 1036–1064.
- Schmid, S., Fügenschuh, B., Kissling, E., Schuster, R., 2004a. TRANSMED Transects IV, V and VI: Three lithospheric transects across the Alps and their forelands. In: *The TRANSMED Atlas: The Mediterranean Region from Crust to Mantle*. Springer Verlag.
- Schmid, S.M., Fügenschuh, B., Kissling, E., Schuster, R., 2004b. Tectonic map and overall architecture of the Alpine orogen. *Eclogae Geol. Helv.* 97 (1), 93–117.
- Schönborn, G., 1999. Balancing cross sections with kinematic constraints: the Dolomites (northern Italy). *Tectonics* 18 (3), 527–545.
- Sharman, G.R., Hubbard, S.M., Covault, J.A., Hirsch, R., Linzer, H.G., Graham, S.A., 2018. Sediment routing evolution in the North Alpine Foreland Basin, Austria: interplay of transverse and longitudinal sediment dispersal. *Basin Res.* 30 (3), 426–447.
- Shipilin, V., Tanner, D.C., von Hartmann, H., Moeck, I., 2020. Multiphase, decoupled faulting in the southern German Molasse Basin—evidence from 3-D seismic data. *Solid Earth* 11 (6), 2097–2117.
- Sinclair, H., 1997a. Flysch to molasse transition in peripheral foreland basins: the role of the passive margin versus slab breakoff. *Geology* 25 (12), 1123–1126.
- Sinclair, H., 1997b. Tectonostratigraphic model for underfilled peripheral foreland basins: an Alpine perspective. *Geol. Soc. Am. Bull.* 109 (3), 324–346.
- Sinclair, H., Naylor, M., 2012. Foreland basin subsidence driven by topographic growth versus plate subduction. *Bulletin* 124 (3–4), 368–379.
- Sinclair, H., Coakley, B., Allen, P., Watts, A., 1991. Simulation of foreland basin stratigraphy using a diffusion model of mountain belt uplift and erosion: an example from the Central Alps, Switzerland. *Tectonics* 10 (3), 599–620.
- Sissingh, W., 1997. Tectonostratigraphy of the North Alpine Foreland Basin: correlation of Tertiary depositional cycles and orogenic phases. *Tectonophysics* 282 (1–4), 223–256.
- Stampfli, G.M., 1993. Le Briançonnais, terrain exotique dans les Alpes? *Eclogae Geol. Helv.* 86 (1), 1–45.
- Stampfli, G., Mosar, J., Marquer, D., Marchant, R., Baudin, T., Borel, G., 1998. Subduction and obduction processes in the Swiss Alps. *Tectonophysics* 296 (1–2), 159–204.
- Stampfli, G., Borel, G.D., Marchant, R., Mosar, J., 2002. Western Alps geological constraints on western Tethyan reconstructions. *J. Virtual Explor.* 8, 77–106.
- Stockmal, G., Colman-Sadd, S., Keen, C., O'Brien, S., Quinlan, G., 1987. Collision along an irregular margin: a regional plate tectonic interpretation of the Canadian Appalachians. *Can. J. Earth Sci.* 24 (6), 1098–1107.
- Strunck, P., Matter, A., 2002. Depositional evolution of the western Swiss Molasse. *Eclogae Geol. Helv.* 95, 197–222.
- Subrahmanyam, D., Rao, P., 2008. Seismic attributes—a review, 7th international conference & exposition on petroleum geophysics. Hyderabad 398–404.
- Supak, S., Bohnenstiel, D., Buck, W., 2006. Flexing is not stretching: an analogue study of flexure-induced fault populations. *Earth Planet. Sci. Lett.* 246 (1–2), 125–137.
- Tetreault, J.A., Buitser, S., 2012. Geodynamic models of terrane accretion: Testing the fate of island arcs, oceanic plateaus, and continental fragments in subduction zones. *J. Geophys. Res.* Solid Earth 117 (B8).
- Trümpy, R., 1960. Paleotectonic evolution of the Central and Western Alps. *Geol. Soc. Am. Bull.* 71 (6), 843–907.
- Tvedt, A.B., Rotevatn, A., Jackson, C.A.-L., Fossen, H., Gawthorpe, R.L., 2013. Growth of normal faults in multilayer sequences: A 3D seismic case study from the Egersund Basin, Norwegian North Sea. *J. Struct. Geol.* 55, 1–20.
- Ustaszewski, K., Schmid, S.M., FÜGENSCHUH, B., Tischler, M., Kissling, E., Spakman, W., 2008. A map-view restoration of the Alpine-Carpathian-Dinaridic system for the early Miocene. *Swiss J. Geosci.* 101, 273–294.
- Van der Meulen, M., Meulenkamp, J., Wortel, M., 1998. Lateral shifts of Apenninic foredeep depocentres reflecting detachment of subducted lithosphere. *Earth Planet. Sci. Lett.* 154 (1–4), 203–219.
- Vogt, K., Gerya, T.V., 2012. From oceanic plateaus to allochthonous terranes: Numerical modelling. *Gondwana Res.* 25 (2), 494–508.
- Vogt, K., Willingshofer, E., Matenco, L., Sokoutis, D., Gerya, T., Cloetingh, S., 2018. The role of lateral strength contrasts in orogenesis: a 2D numerical study. *Tectonophysics* 746, 549–561.
- Von Eynatten, H., Schlunegger, F., Gaupp, R., Wijbrans, J.R., 1999. Exhumation of the Central Alps: evidence from 40Ar/39Ar laserprobe dating of detrital white micas from the Swiss Molasse Basin. *Terra Nova* 11 (6), 284–289.
- Von Hagke, C., Oncken, O., Ortner, H., Cederbom, C., Aichholzer, S., 2014. Late Miocene to present deformation and erosion of the Central Alps—evidence for steady state mountain building from thermokinematic data. *Tectonophysics* 632, 250–260.
- Wagner, L.R., 1998. Tectono-stratigraphy and hydrocarbons in the Molasse Foredeep of Salzburg, Upper and Lower Austria. *Geol. Soc. Lond. Spec. Publ.* 134 (1), 339–369.
- Waschbusch, P.J., Royden, L.H., 1992. Spatial and temporal evolution of foredeep basins: lateral strength variations and inelastic yielding in continental lithosphere. *Basin Res.* 4 (3–4), 179–196.
- Whiting, B.M., Thomas, W.A., 1994. Three-dimensional controls on subsidence of a foreland basin associated with a thrust-belt recess: Black Warrior basin, Alabama and Mississippi. *Geology* 22 (8), 727–730.
- Zaugg, A., Löpfel, R., 2011. 1114 Nesslau. Schweizerische Eidgenossenschaft Bundesamt für Landestopografie Swisstopo.
- Zerlauth, M., Ortner, H., Pomella, H., Adrian Pfiffner, O., Fügenschuh, B., 2014. Inherited tectonic structures controlling the deformation style: an example from the Helvetic nappes of the Eastern Alps. *Swiss J. Geosci.* 107, 157–175.

- Ziegler, P.A., 1990. Geological Atlas of Western and Central Europe, 1. Geological Society Publishing House.
- Ziegler, P., Dèzes, P., 2007. Cenozoic uplift of Variscan Massifs in the Alpine foreland: timing and controlling mechanisms. *Glob. Planet. Chang.* 58 (1–4), 237–269.
- Ziegler, R., Storch, G., 2008. Mammals from the Cyrena Beds of Offenbach (Hesse)-Biostratigraphic correlation. *Neues Jahrbuch Geol. Palaontol.-Abhandlungen* 248 (3), 267–278.
- Ziegler, P.A., Schmid, S., Pfiffner, A., Schönborn, G., 1996. Structure and evolution of the Central Alps and their northern and southern foreland basins. *Mém. Mus. Natl. d'Hist. Nat.* 1993 (170), 211–233.
- Zweigel, J., Aigner, T., Luterbacher, H., 1998. Eustatic versus tectonic controls on Alpine foreland basin fill: sequence stratigraphy and subsidence analysis in the SE German Molasse. *Geol. Soc. Lond. Spec. Publ.* 134 (1), 299–323.